UNCLASSIFIED

SECURITY CLASSIFICATION OF THIS PAGE (When Data Entered)

REPORT DOCUMENTATION PAGE		READ INSTRUCTIONS BEFORE COMPLETING FORM
1. REPORT NUMBER	2. GOVT ACCESSION NO. AD-A116880	3. RECIPIENT'S CATALOG NUMBER
4. TITLE (and Subtitle) METHODS FOR 2-BEAM ARRAY PROCESSING		5. TYPE OF REPORT & PERIOD COVERED technical memorandum
		6. PERFORMING ORG. REPORT NUMBER ARL-TM-82-10
7. AUTHOR(s) Terry L. Henderson		8. CONTRACT OR GRANT NUMBER(s) N00024-79-C-6358
9. PERFORMING ORGANIZATION NAME AND ADDRESS Applied Research Laboratories The University of Texas at Austin Austin, Texas 78712-8029		10. PROGRAM ELEMENT, PROJECT, TASK AREA & WORK UNIT NUMBERS Task 8, Subtask 14
11. CONTROLLING OFFICE NAME AND ADDRESS Naval Sea Systems Command Department of the Navy Washington, DC 20362		12. REPORT DATE 17 May 1982
		13. NUMBER OF PAGES 93
14. MONITORING AGENCY NAME & ADDRESS(if different from Controlling Office)		15. SECURITY CLASS. (of this report) UNCLASSIFIED
		15a. DECLASSIFICATION/DOWNGRADING SCHEDULE

16. DISTRIBUTION STATEMENT (of this Report)

Approved for public release; distribution unlimited.

17. DISTRIBUTION STATEMENT (of the abstract entered in Block 20, if different from Report)

18. SUPPLEMENTARY NOTES

19. KEY WORDS (Continue on reverse side if necessary and identify by block number)

20. ABSTRACT (Continue on reverse side if necessary and identify by block number)

Several methods are considered for using paired beamformers to determine, with high precision or resolution, source geometry and bearing angle. Emphasized are broadband methods and ways of processing the beamformer outputs to effect a proportionality relationship that carries the angular information.

DD FORM 1 JAN 73 1473 EDITION OF 1 NOV 65 IS OBSOLETE

UNCLASSIFIED

SECURITY CLASSIFICATION OF THIS PAGE (When Data Entered)

PAGES _____

ARE

MISSING

IN

ORIGINAL

DOCUMENT

TABLE OF CONTENTS

LIST OF FIGURES

I. INTRODUCTION

Directional hydrophone arrays are often used to determine the physical attributes of a distant source or reflector of acoustic waves. Although the range, velocity, and bearing of the target are often of greatest interest, in many cases it is important to learn as much as possible about its geometric structure, and to determine its precise bearing angle and depression-elevation angle with respect to background objects. A single beamformer may be used for this purpose, but better results can often be obtained by using two beamformers, for example, one having a sharp peak and the other a null at broadside.

Complementary beams have long been known to be useful for precision acoustic or radio direction finding.[1] Although more sophisticated techniques have been developed in recent years,[2,3] 2-beam techniques still have value. They provide a resource that has not yet been exhausted, particularly with regards to broadband signals, and they are much more amenable to performance prediction than other techniques.

In this paper, some familiar 2-beam techniques are extended to the broadband case. In particular, the amplitude comparison concept is extended to a scale comparison method that is applicable to signals of arbitrary spectra and angles of incidence. Moreover, several new results are given that are of interest even in the single frequency case. In contrast to most recent studies, two outputs are produced that are related by a simple proportionality rule rather than by a time delay. This approach makes it possible to use simpler statistical models for the corrupting effects of multipath distortion or complexities of target structure. An appendix is included on phase front distortion as it affects estimates of wave source direction.

The report is written in tutorial style, but it contains several new results and methods. We begin with a review of some basic properties of arrays as seen from a signal processing point of view.

II. SIGNAL PROCESSING CHARACTERISTICS OF A LINE ARRAY BEAMFORMER

Suppose a plane wave, not necessarily sinusoidal, arrives at angle θ as shown in Fig. 1. Note that θ is the angle between the wavefront and the positive x-axis as well as the angle by which the wave source is displaced from broadside aspect. If the instantaneous acoustic pressure at the origin is $p(t)$, then at an arbitrary point along the x-axis, its measured value must be $p[t-(x/c)\sin\theta]$, where c is the speed of propagation. Suppose a receiving aperture with aperture shading function $w(x)$ is used to sense the wave field along the x-axis so as to produce an output

$$q(t) = \int w(x)\, p\left(t - \frac{x}{c}\sin\theta\right) dx \quad . \tag{1}$$

(Integrals with unlabeled limits will be assumed to extend over the range $-\infty$ to $+\infty$.) The aperture shading function $w(x)$ may be effected by the physical characteristics of the receiving transducers, by electronic circuitry, by digital computation, or by a combination of those methods. In any case, the entities that perform the spatial integration of Eq. (8) will be collectively referred to as a beamformer. Used here, this term does not include beamsteering, a processing task that will be neglected in our treatment.

For an aperture of finite length, the function $w(x)$ is zero outside some finite region, and the integration limits can be collapsed to that domain if desired. The shading function $w(x)$ is permitted to take negative values, but the integral of its magnitude must be finite. In the case of a receiving array composed of a finite number of point

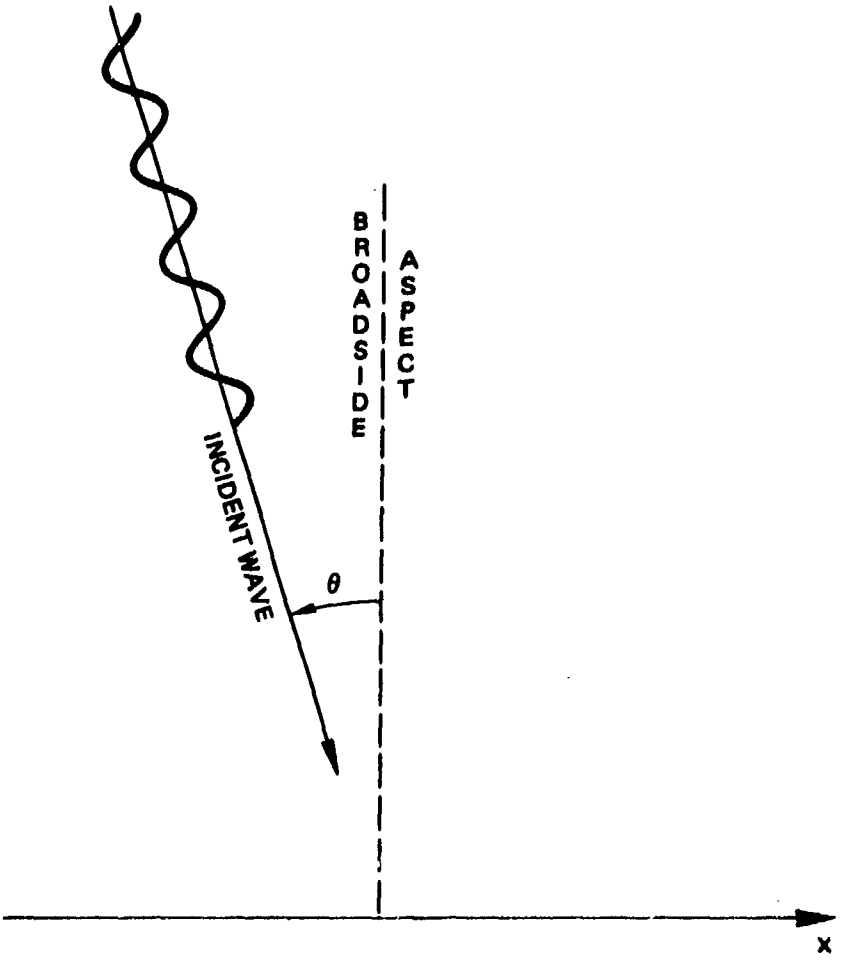

FIGURE 1
INCIDENT WAVE GEOMETRY

ARL:UT
AS-82-781
TLH-GA
5-21-82

transducers, w(x) is just a series of impulses. If we substitute kt for t in Eq. (1), with k defined as $c^{-1}\sin\theta$, the result is

$$q(kt) = \int w(x)\, p[k(t-x)]\, dx = w(t) * p(kt) \quad , \qquad (2)$$

where * denotes convolution. But convolutions obey the following scaling property, as can easily be verified: if f(t)=g(t)*h(t), then

$$f(at) = |a|\, g(at) * h(at) \quad . \qquad (3)$$

Application of this property to Eq. (2) with 1/k as the scalar a and q(kt) as f(t) gives the result

$$q(t) = w_\theta(t) * p(t) \quad , \qquad (4)$$

where the <u>temporal aperture function</u> for direction θ is defined as

$$w_\theta(t) = \left|\frac{1}{k}\right| w\left(\frac{t}{k}\right) = \left|\frac{c}{\sin\theta}\right| w\left(\frac{c}{\sin\theta}\right)t \quad . \qquad (5)$$

This new function may be visualized as an area-preserving projection of w(x) onto a t-axis that is directed along the path of wave propagation (see Fig. 2). The Fourier transforms of w(t) and $w_\theta(t)$ must then obey the relationship $W_\theta(f)=W[(f/c)\sin\theta]$. Furthermore, $W_\theta(f)$ has the constant value M_o when $\theta=0$, where M_o is the area under the curve described by w(x), i.e., it is the "zeroth" moment integral of the aperture shading function. Equation (4) gives the <u>time domain representation</u> of the signal processing function of the beamformer. Taking the Fourier transform gives

$$Q(f) = W_\theta(f)\, P(f) = W\left(\frac{f}{c}\sin\theta\right) P(f) \quad , \qquad (6)$$

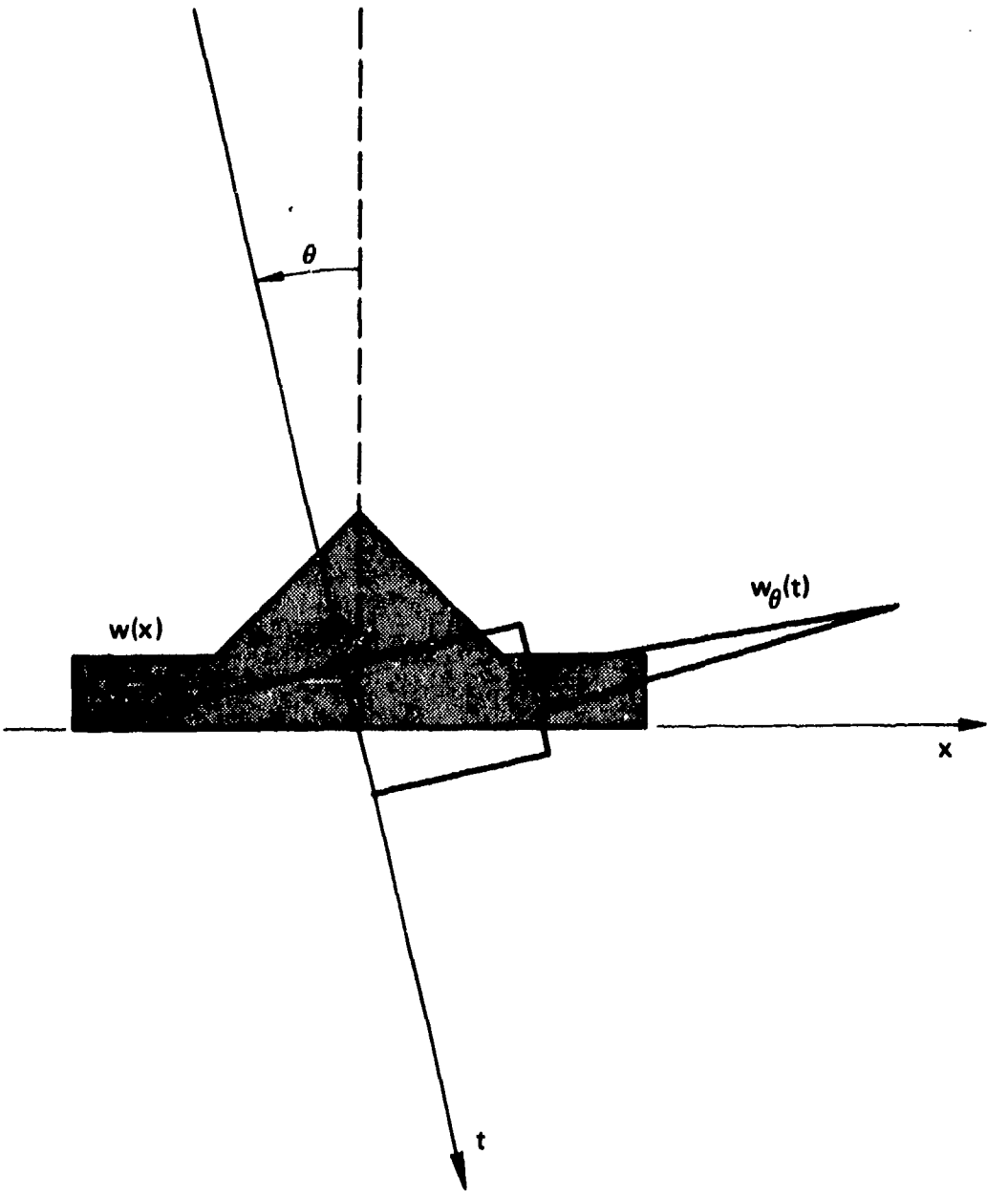

FIGURE 2
TEMPORAL APERTURE FUNCTION

ARL:UT
AS-82-782
TLH-GA
5-21-82

which is the frequency domain representation of the beamformer's signal processing behavior. On the other hand, if Eq. (1) is attacked by expanding $p[t-(x/c)\sin\theta]$ in a power series, i.e.,

$$p\left(t - \frac{x}{c}\sin\theta\right) = p(t) - \sin\theta\,\frac{x}{c}\,\dot{p}(t) + \ldots \quad , \tag{7}$$

then the result is

$$q(t) = M_0 p(t) - \sin\theta\,(M_1/c)\,\dot{p}(t) + \ldots \quad , \tag{8}$$

where the nth term in the series is

$$-\frac{M_n}{n!}(\sin\theta)^n\, c^{-n}\, p^{(n)}(t) \quad , \tag{9}$$

with M_n being the nth moment integral of the aperture,

$$M_n \triangleq \int x^n\, w(x)\, dx \quad . \tag{10}$$

Note that the definition of M_0 is consistent with that given previously, and $W(0)=M_0$. Equation (8) gives the derivative series representation for the signal processing behavior of the beamformer. An important consequence of this representation is that as θ approaches zero (broadside aspect) the output becomes like $M_0 p(t)$, which means that if $M_0 \neq 0$ then the dominant term has no first order dependence upon θ. On the other hand, if $M_0=0$ and $M_1 \neq 0$ then the dominant term in the output is $(M_1/c)\dot{p}(t)\sin\theta \simeq (-M_1/c)\dot{p}(t)\theta$. The resulting first order dependence upon θ of the dominant term makes this type of beamformer useful for estimating the direction of plane waves arriving at near-broadside aspect, if the derivative-taking action of the array is taken into account.

To emphasize the directional characteristic of the output at a particular frequency f_o, it is useful to rewrite Eq. (6) in the form

$$Q(f_o) = K(\theta,f_o)\, P(f_o) \quad , \tag{11}$$

where $K(\theta,f_o)$ is the directivity function for frequency f_o,

$$K(\theta,f_o) \triangleq W[(f_o/c)\sin\theta] \quad . \tag{12}$$

This complex function relates the amplitude and phase of the output component at frequency f_o to that of the incident pressure wave $p(t)$. In particular, if $p(t)$ is a pure sinusoid, i.e.,

$$p(t) = \mathrm{Re}\left\{Pe^{j2\pi f_o t}\right\} \quad , \tag{13}$$

where P is the complex phase amplitude factor, then

$$P(f) = 1/2[P\,\delta(f-f_o) + P^*\delta(f+f_o)] \quad , \tag{14}$$

which, after substituting into Eq. (6) and taking inverse transforms, leads to

$$q(t) = \mathrm{Re}\left\{Qe^{j2\pi f_o t}\right\} \quad , \tag{15}$$

where

$$Q \triangleq K(\theta,f_o)P. \tag{16}$$

Equation (16), used here to define the beamformer output phaser Q, might also be regarded as a working definition of the directivity function $K(\theta,f_o)$, given in terms of the complex envelope of the beamformer output for an incident sinusoidal wave. The directivity function is often expressed with its broadside value normalized, i.e., as $K(\theta,f_o)/M_o$, in

the literature. But this cannot be done if $M_0=0$, i.e., if the area under w(x) is zero, so that the directivity pattern has a null at broadside, and therefore no normalization will be applied here.

It is worth pointing out that Eq. (12) underpins the following well-known interpretation of spectral transforms: any graphical compendium of Fourier transforms may be regarded as a compendium of directivity functions if one merely marks the frequency axis according to the non-linear angular scale $\theta=\arcsin(cf/f_0)$, where f is the frequency variable in the graphical representation of the transform. One needs only that part of the plot for which $|cf/f_0|<1$, i.e., $|f|<f_0/c$.

III. SYMMETRY PROPERTIES

Suppose an aperture shading function $w(x)$ has even symmetry, $w(x)=w(-x)$. Then its odd moment integrals $M_1, M_3, \ldots$, vanish, which implies via the derivative series representation of Eq. (8) that the beamformer output must be composed of $p(t)$ and its even derivatives, with only even powers of θ. The Fourier transform of $w(x)$ is necessarily real-even, which means the directivity function $K(\theta, f_o)$ is real valued and possesses even symmetry with respect to both of the variables θ and f_o. The beamformer output carries no information as to the sign of θ, and all of its sinusoidal components are in phase (allowing for reversed sign) with those of the acoustic pressure at the origin. At broadside aspect the output is relatively insensitive to small variations in the angle of the incidence, exhibiting only a second order dependence on θ.

By similar reasoning, a shading function with odd symmetry, $w(x)=-w(-x)$, has $M_0=M_2=,\ldots,=0$, so its output $q(t)$ is composed of only odd derivatives of $p(t)$ with odd powers of θ, and the Fourier transform of $w(x)$ is imaginary-odd. The directivity function $K(\theta, f_o)$ displays odd symmetry with respect to θ and f_o. The beamformer output reverses in sign whenever the direction angle θ crosses broadside aspect, and at broadside displays a first order sensitivity to θ that is determined by the size of the first moment integral M_1. Every sinusoidal component of the beamformer output $q(t)$ is 90° out of phase with its antecedent component in the incident wave pressure $p(t)$, with the direction of that phase shift depending upon the sign of θ.

Since the odd or even symmetry of the aperture shading function implies a similar symmetry in the directivity function, the terms "odd beamformer" or "even beamformer" are entirely appropriate.

IV. TEMPORAL INTEGRATION OF BEAMFORMER OUTPUT

Equations (4) and (5) can be combined to express the beamformer output more directly for a general aperture shading $w(x)$,

$$q(t) = |k|^{-1}\, w(t/k) * p(t) \quad , \tag{17}$$

where $k=c^{-1}\sin$ as before. Now suppose $q(t)$ is integrated from $-\infty$ to t by an operational amplifier circuit. This temporal integration can be symbolically represented as $u(t)*q(t)$, where $u(t)$ is the unit step function. But

$$u(t) * q(t) = |k|^{-1}\, u(t) * w(t/k) * p(t)$$

$$= |k|^{-1}\, f(t) * p(t), \tag{18}$$

where $f(t) \triangleq u(t)*w(t/k)$. Moreover, the convolution scaling property of Eq. (3) implies that $f(kt)=|k|u(kt)*w(t)$. If we define a new aperture shading function

$$w_c(x) \triangleq \mathrm{sgn}(k)\, u(kx) * w(x) \quad , \tag{19}$$

then $f(t)=kw_c(t/k)$ which, when substituted into Eq. (18), gives

$$u(t) * q(t) = k\, |k|^{-1}\, w_c(t/k) * p(t) \quad . \tag{20}$$

Except for the multiplicative factor k, the right-hand side of this equation has the same form as that of Eq. (17), which means we can rewrite it in the equivalent form of Eq. (1),

$$u(t) * q(t) = k \int w_c(x)\, p\left(t - \frac{x}{c}\sin\theta\right) dx \quad . \tag{21}$$

The upshot is that whenever the output of a beamformer having aperture shading w(x) is passed through an integrating circuit, the resulting signal is identical to what would have been produced by the companion beamformer whose aperture shading $w_c(x)$ is defined in Eq. (19), except that it is multiplied by $k=c^{-1}\sin\theta$. Although the definition of $w_c(x)$ would seem to depend on the angle of arrival through its dependence upon $k=c^{-1}\sin\theta$, it really depends only on the sign of θ, since $u(kx)=u(x)$ if $k>0$, and $u(kx)=1-u(x)$ if $k<0$. It follows that

$$w_c(x) = \int_{-\infty}^{x} w(x)\, dx \tag{22}$$

if $\theta>0$, but

$$w_c(x) = -\int_{x}^{+\infty} w(x)\, dx \tag{23}$$

if $\theta<0$.

If w(x) has odd symmetry, then these two formulas are completely equivalent. Thus to any odd beamformer one can associate a unique, even, companion beamformer whose aperture shading function is just the integral of the odd-symmetric function w(x) from $-\infty$ to x. Odd and even aperture shading functions having this relationship are said to satisfy the "Kerr-Murdock conditions" in the antenna literature.[4,5,6] For a given odd-symmetric shading function, the corresponding even-symmetric shading function so formed will be termed the K-M companion, denoted $w_{KM}(x)$.

Equation (21) makes it possible to determine the performance of an odd beamformer from that of a hypothetical even beamformer. The directional characteristics of an even-symmetric aperture are much more familiar to array designers, and to make the transition to an odd beamformer it is

only necessary to integrate its aperture shading to get the even-symmetric aperture shading of its K-M companion even beamformer, whose directional characteristics will exactly predict those of the odd beamformer except for a temporal integration (which applies a 90° phase shift to each sinusoidal wave component) and a multiplicative factor $k=c^{-1}\sin\theta$ (which gives the beamformer its characteristic odd-symmetric directivity function).

A more important application of this result, however, lies in the design of beamformers for precision direction finding.

V. DIRECTION FINDING BY TRANSFORMS

The Fourier transform relationship between the beamformer output q(t) and the incident wave, represented by the acoustic pressure at the origin, is given by Eq. (6), repeated here for convenience:

$$Q(f) = P(f)\ W\left(\frac{f}{c}\sin\theta\right) \quad . \tag{24}$$

Since q(t) is measured, c is a physical constant, and w(x) is a designer's choice, the only unknowns implicit in Eq. (24) are the incident waveform p(t) and its angle θ. For the rest of this report we shall be concerned with determining the incident wave angle θ.

If p(t) could somehow be divined, then the three transforms Q(f), W(f), and P(f) would need to be computed only once, and θ could be found to achieve equality in Eq. (24). But in practice p(t) is never known beforehand. Even if it is produced as a reflection of a known projected wave (i.e., by active sonar) or by a distant transmitter of known output, then at best one knows $p(t)=Ap_0(t-a)$, where $p_0(t)$ is known but a and A are unknown. Recalling that the magnitude of a Fourier transform is invariant with respect to a time shift, we may conclude from Eq. (24) that

$$|Q(f)| = |A|\ |P_0(f)|\ \left|W\left(\frac{f}{c}\sin\theta\right)\right| \quad , \tag{25}$$

which may be amenable to solving for θ. Since there are two unknowns, |A| and the incident wave angle θ, it is essential to treat at least two frequencies. Unfortunately, the solution for θ will be ambiguous as to

sign, since $|W(f)|$ is an even function when $w(x)$ is real, but the information gained about θ may be useful despite that shortcoming.

The "phase-ignorant" method described above may have some applications, but it is far better to use two beamformers having different aperture shading functions, $w_1(x)$ and $w_2(x)$, that spatially integrate the acoustic field simultaneously along the same measurement axis. In practice, this may be achieved by using two sets of shading resistors for the same array of transducers, by placing two arrays end to end (or even side by side as an approximation), splitting an existing array at the middle, processing the individual transducer outputs in a computer, or by a variety of other means. Thus two outputs, $q_1(t)$ and $q_2(t)$, can be produced, giving two transform equations of the form of Eq. (24), from which the common term $P(f)$ can be eliminated, leaving

$$Q_1(f)\, W_2\left(\frac{f}{c}\sin\theta\right) = Q_2(f)\, W_1\left(\frac{f}{c}\sin\theta\right) \quad , \tag{26}$$

which may be solved for θ.

This <u>computational transform method</u> for direction finding can be summarized as follows. The two beamformer outputs $q_1(t)$ and $q_2(t)$ are Fourier transformed to get $Q_1(f)$ and $Q_2(f)$, which may be evaluated at some set of discrete frequencies (hence, a fast Fourier transform is acceptable). In order to test Eq. (26) for equality at different values of θ, the Fourier transforms, $W_1(f)$ and $W_2(f)$, of the shading functions must be computed with $(f/c)\sin\theta$ substituted for f. This is most easily done if $W_1(f)$ and $W_2(f)$ have relatively simple functional forms comprising algebraic and/or elementary transcendental functions. Then θ can be adjusted to minimize the error of Eq. (26) over an appropriate range of frequencies by any of various criteria, such as minimizing the magnitude-squared equation error. The use of just a single frequency may be sufficient.

Although this method seems straightforward enough, its success will hinge upon such factors as the dissimilarity of the two beamformers, the distribution of signal energy in the frequency spectrum, and the effects of the windowing that are inevitable when computing the Fourier transforms of the beamformer outputs. Just how these factors will affect the results is difficult to determine.

There are ways, however, to extract θ directly from a pair of beamformer outputs. These methods are highly structured and have a more easily predicted performance than the computational transform method. They rely upon the use of specific choices for the aperture shading functions $w_1(x)$ and $w_2(x)$, or upon restrictive assumptions concerning $p(t)$ (e.g., that it is sinusoidal). The balance of this report will be devoted to a study of these methods. However, one should keep in mind that, after performance predictions have been made, there is always the option of analyzing the beamformer output using the computational transform method just described, and perhaps of capitalizing upon the beamformer structure to improve the computational accuracy or to compensate for known imperfections in beamforming.

VI. DIRECTION FINDING BY TIME COMPARISON

If the aperture weighting functions of a pair of beamformers are related by an axial shift, $w_1(x)=w_2(x-A)$, then the beamformer outputs exhibit a differential time shift, $q_1(t)=q_2(t-A\sin\theta/c)$, as may be verified by expressing $q_1(t)$ in the integral form of Eq. (1) and changing the variable of integration to $x'=x-A$. Such beamformers may be termed <u>time comparison</u> beamformers since the direction angle θ of the incident plane wave reveals itself as $\theta=\arcsin(cTA^{-1})$, where T is the relative time shift. Axially shifted aperture weighting functions may be realized quite simply, for example, by splitting a transducer array at the center or by placing two arrays end to end. Procedures for estimating the relative delay between two signals, even in the presence of noise, have been thoroughly treated in the literature (a special issue of the IEEE Transactions on Acoustics, Speech, and Signal Processing was devoted to that subject).[7] A statistical crosscorrelation of the two beamformer outputs may be all that is needed, at least in theory. The problem is not an easy one, however, particularly if the incident wave angle θ varies so rapidly that the analysis must be confined to a brief sample of output data. Although the relationship between the beamformer outputs is linear, it is not memoryless. Moreover, if the incident wave is periodic with period T_o, then T can be determined only to within an unknown integer multiple of T_o, resulting in ambiguous solutions for θ, unless $A<T_oc$.

Since this ground has been explored extensively by many investigators, we shall confine our attention to pairs of beamformers that exhibit a linear, memoryless relationship between their outputs.

VII. DIRECTION FINDING BY SCALE COMPARISON

Consider an odd-even pair of beamformers whose aperture shading functions satisfy the Kerr-Murdock conditions, where $w_1(x)$ is the odd-symmetric aperture shading function and

$$w_{KM}(x) = \int_{-\infty}^{x} w_1(x)\, dx \quad . \tag{27}$$

As previously shown, the temporally integrated output of the odd beamformer,

$$\bar{q}_1(t) \triangleq u(t) * q_1(t) = \int_{-\infty}^{t} q_1(t)\, dt \quad , \tag{28}$$

is related to the unintegrated output of the even (K-M companion) beamformer by

$$\bar{q}_1(t) = kq_{KM}(t) = c^{-1} \sin\theta\, q_{KM}(t) \quad . \tag{29}$$

Thus, the incident wave angle θ can be determined unambiguously over the range $-\pi/2$ to $+\pi/2$ by finding the factor k that relates the beamformer outputs and then setting $\theta=\arcsin(kc)$. Interestingly, if the wave is presumed to have come from some remote point at range d, then the displacement of that point from the broadside plane (i.e., the crossrange) is just kcd, as follows from elementary trigonometry. Determining the value of k can be as simple as dividing $\bar{q}_1(t)$ by $q_{KM}(t)$, provided that:

(1) the signal-to-noise ratio (S/N) is very large,

(2) the incident wave is truly planar, and

(3) the beamformers have been implemented with no compromises in aperture shading.

The use of an X-Y oscilloscope display is particularly appropriate for determining the scaling factor that links the two signals.

Figure 3 gives several possible pairs of aperture shading functions that satisfy the Kerr-Murdock conditions, but in practice they may be difficult to realize precisely. The easiest way to create an odd-even beamformer pair with outputs $q_1(t)$ and $q_2(t)$ is to choose an even aperture shading function, split the aperture at the center to form separate left and right outputs, and then take $q_1(t)$ as the difference of those outputs and $q_2(t)$ as the sum. In that case, $w_2(x)=\pm sgn(x)w_1(x)$. Indeed, any pair of beamformers designed for the time comparison technique discussed previously can be converted to such an odd-even pair by this sum-and-difference method. Unfortunately the only odd-even pair of shading functions that satisfies both the Kerr-Murdock condition and the split aperture condition, i.e., for which $w_1(x)=\pm sgn(x)w_{KM}'(x)$, is the exponential pair given in Fig. 3, which requires a line array of infinite length (admittedly, the exponential aperture might be approximated by one of finite length). Even if one is willing to forego the simplicity of a split aperture beamformer, it must be appreciated that the Kerr-Murdock conditions can never be satisfied exactly with a finite line array of discrete transducers.

Fortunately, in most applications it is not essential that the Kerr-Murdock conditions be satisfied perfectly, as will be demonstrated in the next section. Before proceeding we observe that, due to the integral relationship between $w_1(x)$ and $w_{KM}(x)$, their Fourier transforms are related by

$$W_1(f) = j2\pi f W_{KM}(f) \quad , \tag{30}$$

and their moment integrals $M_{1,n}$ and $M_{KM,n}$ obey

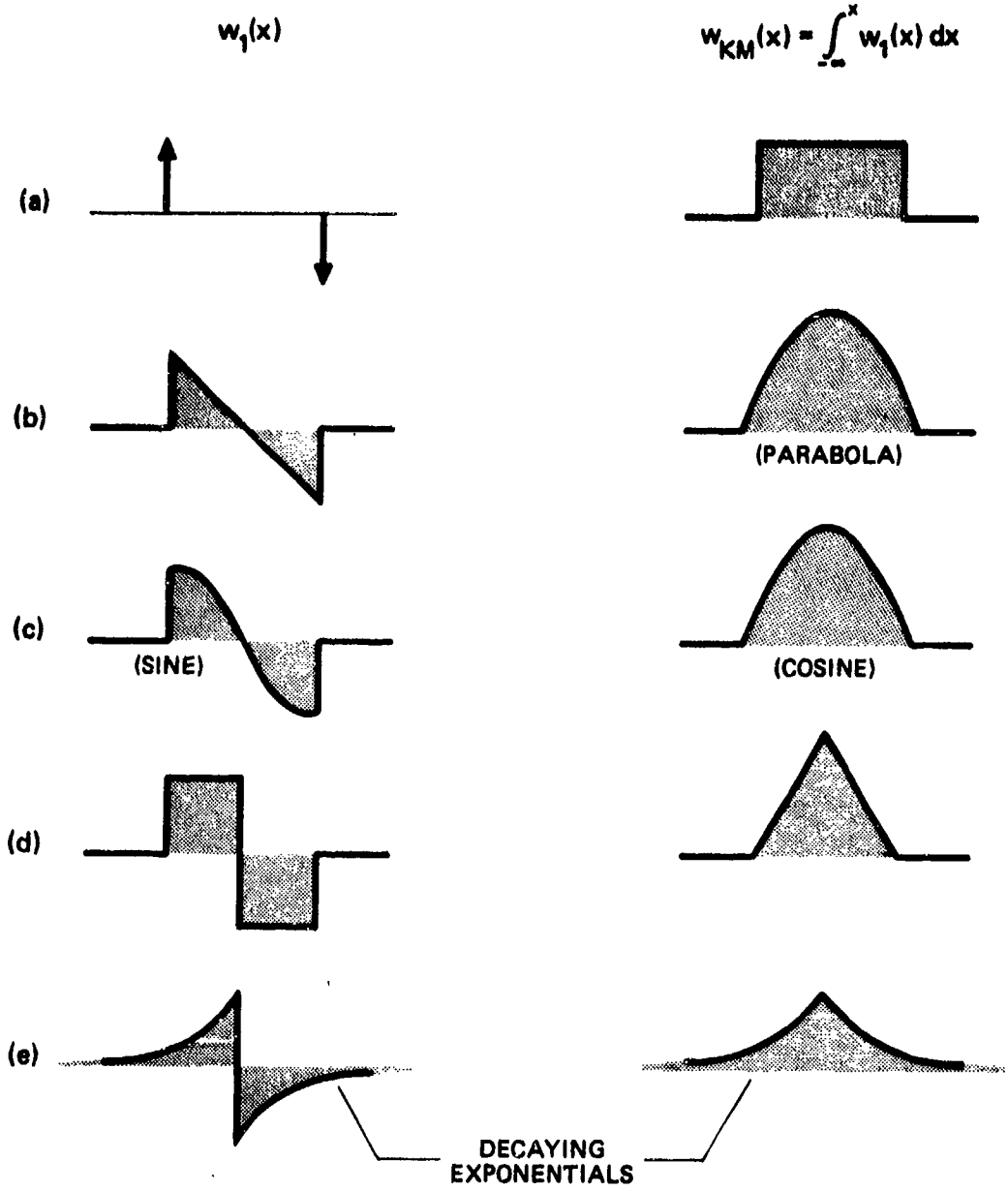

FIGURE 3
APERTURE SHADING FOR KERR-MURDOCK COMPANION BEAMFORMERS

ARL:UT
AS-82-783
TLH-GA
5-21-82

$$M_{1,n+1} = -(n+1)M_{KM,n} \quad . \tag{31}$$

The latter result follows easily from integration by parts.

VIII. USING A GENERAL ODD-EVEN BEAMFORMER PAIR

We will consider if it is possible to find an even beamformer other than the K-M companion beamformer whose output is proportional to the temporally integrated output of a given odd beamformer through some angle dependent, real valued, scalar factor R. This proposition can be put into equation form, $\bar{q}_1(t)=Rq_2(t)$, where the subscripts 1 and 2 denote the odd and even beamformers, respectively, and can also be expressed in terms of Fourier transforms as

$$(j2\pi f)^{-1} Q_1(f) = RQ_2(f) \quad . \tag{32}$$

With the aid of Eq. (26), this equation may be solved for R,

$$R = \frac{W_1\left(\frac{f}{c}\sin\theta\right)}{j2\pi f W_2\left(\frac{f}{c}\sin\theta\right)} \quad . \tag{33}$$

The use of Eq. (30) gives the equivalent form

$$R = \frac{\sin\theta}{c} \frac{W_{KM}(f')}{W_2(f')} \quad , \tag{34}$$

where $f' \triangleq (f/c)\sin\theta$. Clearly the only way that R can depend upon the wave's angle but not its frequency is for the function $W_2(f)$ to be identical to $W_{KM}(f)$ or a scalar multiple of it. Since equality of the Fourier transforms implies equality of $w_2(x)$ and $w_{KM}(x)$, our question is answered in the negative, at least for an incident wave of unknown, unrestricted

form. No beamformer, nontrivially distinct from the K-M companion beamformer, achieves the desired result for all incident waves.

But if the frequency spectrum of the incident wave is restricted, then Eq. (34) need not be satisfied at all values of f and θ. In the important special case where the incident wave is a sinusoid of frequency f_o, the equality is satisfied automatically, since from Eqs. (33) and (34)

$$R(\theta) = \frac{\sin\theta}{c} \frac{W_{KM}(f')}{W_2(f')} = \frac{K_1(\theta,f_o)}{j2\pi f_o K_2(\theta,f_o)} \quad , \tag{35}$$

using the directivity function notation defined earlier. The scalar factor $R(\theta)$ is clearly an odd-symmetric, real valued function, as can be seen by examining each of the functions in Eq. (35).

In fact, the beamformer outputs will be related by a scalar factor even in the nonsinusoidal case, provided the wave is incident at near-broadside angle. This reasoning follows from the derivative series representations of $q_1(t)$ and $q_2(t)$,

$$q_1(t) = -\sin\theta\left(\frac{M_{1,1}}{c}\right)\dot{p}(t) + \ldots \quad , \tag{36}$$

$$q_2(t) = M_{2,0}\, p(t) + \ldots \quad , \tag{37}$$

which, after integrating the first, combine to give the following proportionality law that is valid for small θ,

$$\bar{q}_1(t) \cong \frac{-\sin\theta}{c}\left(\frac{M_{1,1}}{M_{2,0}}\right) q_2(t) \quad . \tag{38}$$

The angular range over which this simple proportionality applies can be

determined from the frequency domain requirement of Eq. (34). Let A denote the maximum argument, for which $W_{KM}(f)/W_2(f)$ is approximately constant, i.e., if $|f|<A$, then $W_{KM}(f)/W_2(f) \cong W_{KM}(0)/W_2(0) = M_{KM,0}/M_{2,0} = -M_{1,1}/M_{2,0}$ by Eq. (31). Notice that the size of A depends upon how closely the even beamformer approximates the K-M companion beamformer, being quite large if the approximation is good. Now, let f_{max} denote the largest frequency for which the incident wave has significant spectral energy. Then Eq. (34) admits the approximation

$$R \cong \frac{\sin\theta}{c}\left(\frac{-M_{1,1}}{M_{2,0}}\right) \tag{39}$$

over the angular range $|\sin\theta|<cA/f_{max}$. Thus, R is shown to be angle dependent but frequency independent within the limits of this approximation.

These results can be summarized briefly. A proportionality rule,

$$\bar{q}_1(t) = R(\theta)\, q_2(t) \quad , \tag{40}$$

holds between the temporally integrated output of an odd beamformer and the output of an even beamformer, subject to following restrictions:

Case 1: If the even beamformer is the K-M companion to the odd beamformer, then the rule holds for any incident wave and for all θ, with $R(\theta)=k=c^{-1}\sin\theta$.

Case 2: If the incident wave is sinusoidal with frequency f_0, the rule holds for all angles, for any odd-even pair of beamformers, with $R(\theta)$ given by Eq. (35).

Case 3: If the incident wave is nonsinusoidal, the rule still holds for any odd-even beamformer pair, but only for angles near broadside,

$|\theta| < \arcsin(cA/f_{max})$, where the parameters A and f_{max} are defined just prior to Eq. (39).

Once R is determined, the wave angle $-\pi/2 < \theta + \pi/2$ can be unambiguously determined in Case 1, since $\sin\theta$ is monotonic over that range. The same principle applies to Case 3 over a restricted angular range as specified. But in Case 2 the dependency of R upon θ is complicated by the nonconstant ratio term, and $R(\theta)$ will probably not be monotonic over the entire range $-\pi/2 < \theta < +\pi/2$. Thus the unambiguous direction-finding capability will be limited to the angular range over which $R(\theta)$ is monotonic. However, for all of the cases listed above, it will be impossible to determine the proportionality factor R whenever the wave is incident at such an angle that the even beamformer output $q_2(t)$ is too weak to be measured accurately. Hence the angular range will be constrained, for practical purposes, by the beam pattern of the even beamformer.

Integrating the odd beamformer output to make it proportional to the even beamformer output offers a possible benefit even when the transform method is used. The transforms $Q_1(f)$ and $Q_2(f)$ in Eq. (26) will be distorted by the inevitable windowing effects of a computational Fourier transform, and an imbalance may thus result due to the dissimilarity of $q_1(t)$ and $q_2(t)$. If $q_1(t)$ is integrated before digital sampling, however, the windowing effects will be balanced. Thus $Q_1(f)$ in Eq. (26) may be replaced by $(j2\pi f)^{-1}\overline{Q}_1(f)$, where $\overline{Q}_1(f)$ denotes the computed Fourier transform of $\overline{q}_1(t)$.

IX. RELATED PROCESSING TECHNIQUES

Those familiar with radar systems will have noticed that, when restricted to sinusoidal waves, much of what has been presented here strongly resembles the type of signal processing performed by a monopulse radar. The same processing method was used successfully in the bearing deviation indicator (BDI) that was developed at Harvard Underwater Sound Laboratory during World War II.[8] This instrument, which sensed the bearing angle of sonar echoes from a hostile submarine, was perfected prior to the development of monopulse radar. Although long since declassified, the BDI project received little attention in the open literature. In sharp contrast, monopulse radar has been elaborated and extended by numerous papers[9] and at least one book.[6]

Among other things, our treatment extends to general, nonsinusoidal waves. This may not seem pertinent to many applications, for example to active sonar systems that employ sinusoidal "pings," however, it is actually important in even that case when one must ponder the effects upon bandwidth of using short pulse durations and tuned filters. It is significant that an integrator, as we have shown, provides the proper mechanism to extend the traditional 90° phase shift operation to broadband signals (rather than a Hilbert transform, for example), when coupled with the use of odd-even shading functions that satisfy the Kerr-Murdock conditions. To the author's knowledge, the radar literature contains no references to the use of the Kerr-Murdock conditions for anything other than providing a "linear" (with respect to $\sin\theta$) sensed angle output, for waves of a single frequency.

Although restricted to sinusoidal waves, the monopulse literature includes error effect studies,[10] statistical analyses,[11] performance data,[12]

and design criteria that may be of considerable value in predicting the performance of paired beamformers used in direction finding. To acquaint the reader with monopulse techniques and terminology, and to make the monopulse literature more accessible, the following detailed summary is provided. The reader is hereby cautioned that transitions between the sonar and radar environments will be made without comment.

The term monopulse[6] is used to describe radar and radio tracking systems that measure a target's azimuth and/or elevation angle after receiving just one pulse of radio frequency (RF) energy, in contrast to systems that scan the target by slowly rotating the antenna, by wobbling some component of the antenna, or by sequentially switching between elements of a compound antenna. In the monopulse method separate beams are used. They are either pointed in the same direction with displaced phase centers ("phase comparison" or "interferometric"), or aimed in slightly different directions separated by a squint angle ("amplitude comparison"). The dual beams may be obtained from paired antennas, or by merely employing two RF feedpoints.

Monopulse radar was developed primarily to circumvent a fault of scanners, namely that modulations produced by scanning are similar to the modulations produced by target fluctuations, resulting in possible confusion or interference. But the monopulse method quickly gained a reputation for remarkably precise measurements of target direction under good signal-to-noise ratio (S/N) conditions. The technique has given single target tracking performance with angular precision that bettered the Rayleigh resolution criterion by 2000 to 1 (only 200 to 1 if all system errors and biases were included.)[12] As a device for precision direction-finding, the monopulse radar is the most primitive member of a family of advanced nonlinear processing methods that includes super-resolution techniques, product arrays, maximum likelihood and maximum entropy processing, adaptive null steering, and autoregressive or Prony-type analysis of angular spectra. Yet it is the only method that has found such widespread use in operational radar systems as a means of

extending angular precision beyond the classical limits of linear array processing.

Since digital computers were not yet available when the monopulse method was developed, estimates of target angle had to be computed with simple electronic circuitry, and that fact largely determined which statistic would be computed. Most monopulse systems were designed to compute the real part of the ratio of the complex envelopes of the difference and sum of the outputs of a pair of slightly displaced beams (the difference signal having been delayed by 90° in the case of phase comparison monopulse). This quantity is proportional to the target angle over a limited range.

Although monopulse radars typically measure both azimuth and elevation angles, for simplicity let us consider only the measurement of a single target angle θ, and assume that the target is confined to the same plane that contains a pair of identical line arrays used to observe it. For phase comparison monopulse, these receiving subarrays are collinear but their centers are displaced by a small distance $2h$. For amplitude comparison monopulse, they have a common center but their axes are separated by a small angle $2\theta_s$, where θ_s is called the squint semiangle (i.e., half the squint angle that separates the beams). The left and right outputs $q_L(t)$ and $q_R(t)$ are formed by identical, real-symmetric shading functions. The polar coordinate axis for measuring target angle θ is oriented as shown in Fig. 1. As a consequence of this orientation, $q_L(t)=q_R(t)$ whenever the target is located at $\theta=0$.

Recall from Eq. (16) that the directivity function of a line array beamformer, $K(\theta,f_o)$, expresses the amplitude and phase relationship between the sinusoidal field at the center of an array $p(t)$ and its output $q(t)$,

$$Q = K(\theta,f_o)P \quad , \tag{41}$$

in which P and Q are the phasors associated with p(t) and q(t), and θ is the target angle with respect to the array's broadside aspect. If this equation were applied without modification to both component subarrays of a monopulse system, an incompatibility in the coordinate reference would result. In phase comparison monopulse, the subarray centers are not coincident, and therefore the P's would be different. In amplitude comparison monopulse, the centers are coincident, but the coordinate axes for θ would disagree due to the angular separation. The necessary modification is simple. Let $K(\theta)$ denote the directivity function that both subarrays would have if they were hypothetically coincident (i.e., if h=0 or θ_h=0). We have suppressed the notational dependence of K upon f_o for convenience. Recall from Eq. (12) that $K(\theta)=W[(f_o/c)\sin\theta]$, where W(f) is the real, even-symmetric Fourier transform of w(x), the aperture shading function common to the hypothetically coincident subarrays. But suppose we continue to let P represent the phasor associated with the field p(t) at the coordinate origin, even after the subarrays are separated or squinted. Then if Q_L and Q_R are the phasors associated with the subarray outputs $q_L(t)$ and $q_R(t)$, we have for amplitude comparison monopulse

$$Q_L = K(\theta-\theta_h)P = K(\theta_h-\theta)P \quad , \tag{42}$$

$$Q_R = K(\theta_h+\theta)P \quad , \tag{43}$$

while for phase comparison monopulse,

$$Q_L = e^{jB}\, K(\theta)P \quad , \tag{44}$$

$$Q_R = e^{-jB}\, K(\theta)P \quad , \tag{45}$$

where $B \triangleq 2\pi f_o c^{-1} h \sin\theta$, which is the phase shift due to displacement of the subarray center by distance h.

The transformation to the sum-and-difference outputs $q_1(t)=q_L(t)-q_R(t)$ and $q_2(t)=q_L(t)+q_R(t)$ is obviously invertible, so these

outputs can be used for all subsequent signal processing with no loss of information. If Q_1 and Q_2 denote their phasors, then $Q_1=K_1(\theta)P$ and $Q_2=K_2(\theta)P$, where

$$K_1(\theta) \triangleq K_L(\theta) - K_R(\theta) \quad , \tag{46}$$

$$K_2(\theta) \triangleq K_L(\theta) + K_R(\theta) \quad . \tag{47}$$

For phase comparison monopulse,

$$K_1(\theta) = K(\theta)\, e^{jB} - K(\theta)\, e^{-jB} = 2jK(\theta)\, \sin B \quad , \tag{48}$$

$$K_2(\theta) = K(\theta)\, e^{jB} + K(\theta)\, e^{-jB} = 2K(\theta)\, \cos B \quad , \tag{49}$$

which are real-even and imaginary-odd, respectively. These results are unsurprising since the displaced subarrays are still collinear, so the system may be regarded as a single line array with a pair of beamformers that have aperture shading functions

$$w_1(x) = w(x+h) - w(x-h) \quad , \tag{50}$$

$$w_2(x) = w(x+h) + w(x-h) \quad . \tag{51}$$

Since $w(x)$ is even, $w_1(x)$ and $w_2(x)$ are odd and even, respectively. One of the outputs $q_1(t)$ or $q_2(t)$ must be subjected to a 90° phase shift to bring them into phase agreement. If we use the symbol $\hat{J}$ to represent the 90° phase shift operator, which may be implemented in a variety of ways for sinusoidal signals, then from Eqs. (48) and (49) $q_1(t)=\hat{J}\tan B\, q_2(t)$. Since $\hat{J}2\pi f_0 \bar{q}_1(t)=q_1(t)$ for a sinusoid, recalling that $\bar{q}_1$ denotes the integral of q_1, it follows that a phase comparison monopulse system with sum-and-difference processing constitutes our Case 2 odd-even beamformer pair, for which $\bar{q}_1(t)=R(\theta)q_2(t)$. Clearly,

$$R(\theta) = (2\pi f_o)^{-1} \tan B = (2\pi f_o)^{-1} \tan(2\pi f_o h c^{-1} \sin\theta) \quad . \qquad (52)$$

For this case, the angle can always be determined unambiguously from $R(\theta)$ over the range $|\sin\theta| < c/4f_o h$.

On the other hand, for amplitude comparison monopulse

$$K_1(\theta) = K(\theta_s - \theta) - K(\theta_s + \theta) \quad , \qquad (53)$$

$$K_2(\theta) = K(\theta_s - \theta) + K(\theta_s + \theta) \quad . \qquad (54)$$

These directivity functions are real-even and real-odd, so instead of being 90° out of phase, the outputs are exactly in phase. This departure from the behavior of odd-even beamformers should have been expected, since the component subarrays are not collinear. However, it is true that

$$q_1(t) = \left[\frac{K_1(\theta)}{K_2(\theta)}\right] q_2(t) \quad , \qquad (55)$$

where the quantity in brackets, being a ratio of odd and even real functions, is itself an odd function, monotonic over some angular range, and linear for small θ. Thus θ can be determined from the scalar factor that relates q_1 and q_2, without the need for integrating.

For a single incident wave, the ratio Q_1/Q_2 (or Q_1/jQ_2 in the case of phase comparison radar) ought to be real. However, due to a variety of corruptive effects, it may possess an imaginary part. It is customary to use the real part of the ratio for angle detection, i.e., to use

$$r = \mathrm{Re}\left[\frac{Q_1}{Q_2}\right] \quad \text{or} \quad \mathrm{Re}\left[\frac{Q_1}{jQ_2}\right] \quad . \qquad (56)$$

The implications of this custom will be discussed in a later section of this report.

Before concluding this summary of monopulse radar, we should alert the reader to the fact that some phase comparison systems compare the phases of $q_1(t)$ and $q_2(t)$ directly without ever forming the sum-and-difference signals, and primitive amplitude comparison systems sometimes detect the amplitudes separately before comparison. Note that this latter method is not strictly equivalent to sum-and-difference processing. Moreover, the literature gives considerable attention to various ways of transforming the signals prior to detection, mostly based on the following two simple properties of complex variables: If Z_1 and Z_2 are complex phasors which have equal amplitude but which differ in phase by an angle θ, then $j(Z_1+Z_2)$ and Z_1-Z_2 have like phase but differ in amplitude and have the ratio $\tan(\theta/2)$. On the other hand, if Z_1 and Z_2 have like phase but possess an amplitude ratio r, then Z_1+jZ_2 and Z_1-jZ_2 have like amplitude but differ in phase by $2\arctan(r)$.

X. PHASE SHIFT SQUINTED, AMPLITUDE COMPARISON MONOPULSE VERSUS ODD-EVEN BEAMFORMING

In a sonar implementation of an amplitude comparison monopulse system, it is likely that the beam squinting would be implemented by electronic phase shift steering of a single line array rather than by using two physically distinct arrays. For this case, and with the proper interpretation, there is an equivalence to the use of an odd-even beamformer pair.

The output $q(t)$ of a simple array with an even-symmetric aperture shading function $w(x)$ is, from Eq. (1),

$$q(t) = \int w(x)\, p\left(t - \frac{x}{c} \sin\theta\right) dx \quad .$$

If the complex function $P(x)$ expresses the amplitude/phase of the incident sinusoidal field at point x, and Q is the output phasor, then

$$Q = \int w(x)\, P(x)\, dx \quad . \tag{57}$$

The array can be steered to any angle θ_s by applying a progressive phase shift along the array sensor axis:

$$Q = \int w(x)\, e^{-jSx}\, P(x)\, dx \quad ,$$

$$= \int w(x)\, \cos(Sx)\, P(x)\, dx - j \int w(x)\, \sin(Sx)\, P(x)\, dx \quad , \tag{58}$$

where $S=(f_0/c)\sin\theta_s$. If an amplitude comparison monopulse system is then formed by taking sum-and-difference outputs Q_1 and Q_2 after phase shift steering to the two squinting angles $\theta_s=\pm\theta_h$, the result is

$$Q_1 = -j\int w_1(x)\, P(x)\, dx \quad , \tag{59}$$

$$Q_2 = \int w_2(x)\, P(x)\, dx \quad , \tag{60}$$

where the odd-even shading functions w_1 and w_2 are

$$w_1(x) = 2w(x)\, \sin\left(\frac{x}{c} f_o \sin\theta_h\right) \tag{61}$$

$$w_2(x) = 2w(x)\, \cos\left(\frac{x}{c} f_o \sin\theta_h\right) \quad . \tag{62}$$

From Eq. (60) we see that

$$q_2(t) = \int w_2(x)\, p\left(t - \frac{x}{c}\sin\theta\right) dx \quad . \tag{63}$$

A similar result holds for Eq. (59) except that we must insert the previously defined symbol $\hat{J}$ to account for the 90° phase shift that is implied by the j factor:

$$\hat{J}q_1(t) = \int w_1(x)\, p\left(t - \frac{x}{c}\sin\theta\right) dx \quad . \tag{64}$$

Examination of Eqs. (63) and (64) reveals the phase shift squinted, amplitude comparison monopulse system to be equivalent to an odd-even pair of beamformers, except that it already has a 90° phase shift in its $q_1(t)$ output. But that phase shift was effected artificially as part of the

phase shift steering process, and could just as well have been postponed until needed to bring the sum-and-difference outputs into phase agreement. Thus the difference between these two methods is one of interpretation. The situation is quite different with a true amplitude comparison system, which performs its 90° phase shift by spatial processing rather than electronic or computational processing.

XI. THE PARTICLE MOTION EQUIVALENCE PRINCIPLE

The output $q_2(t)$ of an even beamformer is related to the incident wave by Eq. (4), $q_2(t)=w_{2,\theta}(t)*p(t)$, where $w_{2,\theta}(t)=\left|\frac{1}{k}\right|w_2(t/k)$, with $k=\sin\theta/c$. Suppose the even-symmetric shading fuction $w_2(x)$ has been selected to yield a highly directive broadside beam. Then $W_2(f)$ must mimic the frequency response of a low pass filter if the directivity function $K_2(\theta,f)=W_2[(f/c)\sin\theta]$ is to pass only those waves having small θ. Equation (6) gives the frequency domain behavior, $Q_2(f)=W_2[(f/c)\sin\theta]P(f)$, by which the beamformer may be characterized as an angle dependent low pass filter whose cutoff frequency is inversely proportional to $\sin\theta$, or as an angular filter whose small angle cutoff, i.e., beamwidth, is inversely proportional to frequency. This spatial filter is remarkable in being devoid of phase shift at all frequencies, since $W(f)$ takes only real values. Let f_L denote the low pass cutoff frequency, so that $|W(f)-W(0)|<\delta$ for $|f|<f_L$, where the tolerance parameter δ may be chosen to fit the 3 dB point, for example. We define broadside window as the set of frequency and angle combinations for which

$$\left|\frac{f}{c}\sin\theta\right| < f_L \quad . \tag{66}$$

Thus, if an incident wave "passes through" this window, i.e., if all of its spectral energy is at frequencies that satisfy Eq. (66), then $Q_2(f) = W_2[(f/c)\sin\theta]P(f) \cong W_2(0)\ P(f)$ and it follows that

$$q_2(t) \cong W_2(0)\ p(t) \quad . \tag{67}$$

(For simplicity we shall drop the approximation symbol.) Figure 4 illustrates the windowing effect of the even beamformer's directivity

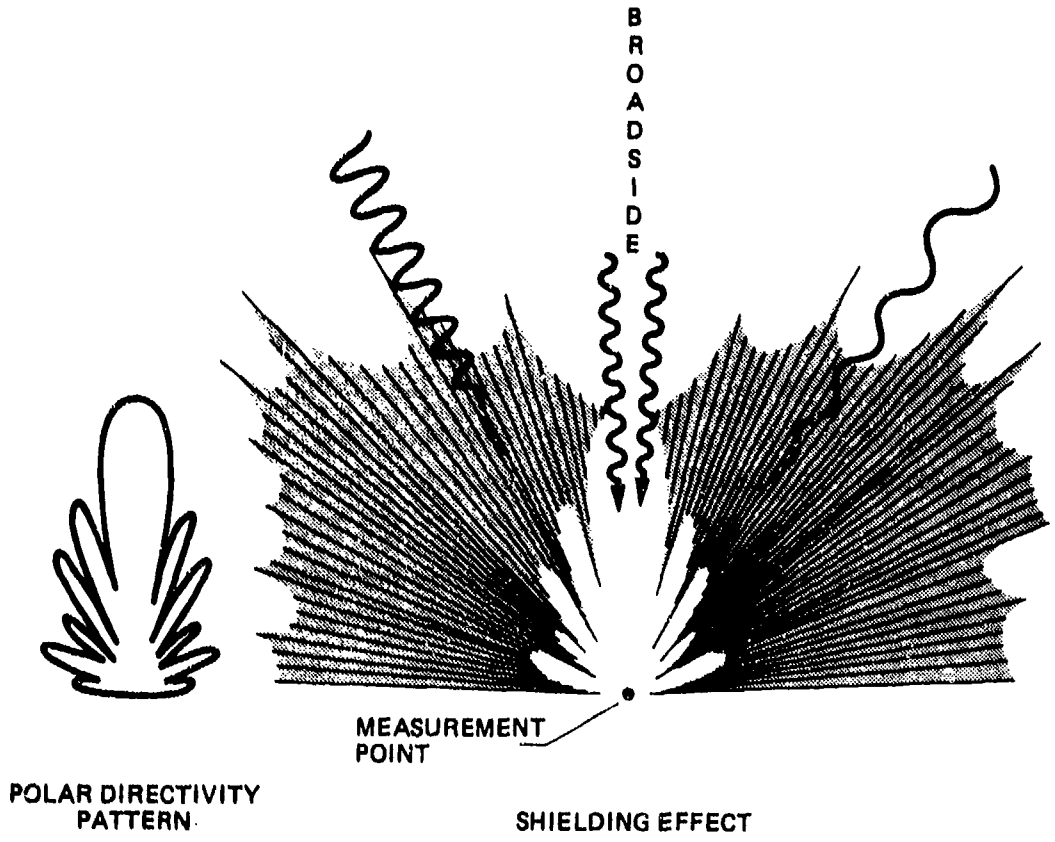

FIGURE 4
SHIELDING EFFECT OF THE EVEN BEAMFORMER

ARL:UT
AS-82-784
TLH - GA
5 - 21 - 82

function upon waves coming from sources at various angles. The effect may be regarded as a shielding action. This figure must be interpreted with caution since the opacities of the directional response are represented only figuratively, with no frequency dependence shown.

Now suppose this even beamformer is combined with its K-M companion beamformer to form an odd-even pair. Also, for the moment, let us restrict our discussion to "plane" waves emanating from very distant wave centers that lie in a single X-Y plane that contains the receiving aperture. If a(t) denotes the acoustic particle displacement along the ray path of a solitary incident plane wave, then $p(t)=-(B/c)\dot{a}(t)$, where B denotes the bulk modulus. The scaling of the aperture shading function $w_2(x)$ is arbitrary, so assume for mathematical convenience that it is scaled to make $W_2(0)=-(c/B)$. With this calibration adjustment the beamformer output for a solitary plane wave incident at angle θ is given by $q_2(t)=\dot{a}(t)$, provided the wave passes through the broadside window unscathed. (Note that we are assuming a line array of acoustic pressure sensors that accurately measure the instantaneous pressure of any plane wave arriving within its broadside window.) It follows that the particle displacement could be determined merely by integrating $q_2(t)$, i.e.,

$$a(t) = \bar{q}_2(t) \quad . \tag{68}$$

To represent the acoustic particle motion on an X-Y display device such as an oscilloscope, it would be necessary to set $Y=a(t)\cos\theta$ and $X=-a(t)\sin\theta$. Recall that

$$\bar{q}_1(t) = \frac{\sin\theta}{c} q_2(t) \quad ,$$

so we may simply set

$$X = -c\bar{\bar{q}}_1(t) \quad , \tag{69}$$

where the double bar denotes two temporal integrations. Unfortunately, there is no linear way to form $Y=a(t)\cos\theta$ without prior knowledge of θ, but if the broadside window admits only waves whose angles are small enough that $\cos\theta$ is approximately one, then we can set

$$Y = \bar{\bar{q}}_2(t) \quad . \tag{70}$$

Notice that the error in setting $\cos\theta=1$ is at most 10% for angles less than 25°, or 1% for angles less than 8°, so the distortions in the display will be quite small in most cases of interest.

For a solitary incident wave, the particle motion (actual or simulated) occurs along a straight line that points toward the wave center, presumed to be an infinite distance away. But this display continues to accurately represent the particle motion at the point of measurement even when several distinct waves with arbitrary spectra arrive from a variety of angles near broadside. This is true because the process of beamforming, scaling, and integration is just as subject to linear superposition as is the acoustic medium itself. Note also that the integrations are reversible, so the display preserves all of the information contained in the beamformer outputs. The eye will likely not be able to interpret that information as well as an electronic angle detector of good design. The subject of angle or slope detection will be covered later. For the moment we simply note that, loosely speaking, the angle of a dominant wave in a background of weaker waves is revealed by the predominant direction of particle motion.

Any odd-even beamformer pair may also be used to generate the display, provided the incident waves have acceptable frequency spectra and angles sufficiently near broadside so that $\bar{\bar{q}}_1(t)=R(\theta)q_2(t)$, and so that $R(\theta)$ accurately approximates $(\sin\theta)/c$ to within a multiplicative factor. The X variable must be properly scaled to compensate for that factor, of course. Moreover, it may be possible to design a substitute beamformer whose output is related to that of the original even

beamformer by the factor cosθ over a limited frequency range. This would reduce the distortion that results from using $q_2(t)$ to drive the Y variable.

The significance of the argument just presented goes beyond the mere generation of an interesting display. It demonstrates that the beamformer outputs contain no more and no less information than is required to describe the acoustic particle motion at a hypothetical measurement point that is shielded by the directivity function associated with the even beamformer. Nothing can be determined about the individual waves, or about the locations of their wave centers, that does not reveal itself in the acoustic motion of this single particle. The problem of properly interpreting the beamformer outputs can be approached purely from the standpoint of basic physics and signal geometry, with little regard to the parameters of the line array that might be used to obtain them.

The <u>particle motion equivalence principle</u> just stated clarifies the role of directivity in identifying the geometrical configuration of a distant cluster of wave centers. The direction of a solitary wave center can always be determined with infinite precision in the absence of measurement noise. But if waves with similar frequency spectra arrive from a cluster of wave centers whose angular extent falls well within the broadside window, then it may not be possible to separate their effects upon particle motion. Nevertheless, analysis of its motion may provide some information about the cluster, and it would seem that such knowledge could only be enhanced by sharpening the directivity function. But unless the directivity can be improved to such a degree that the broadside window masks some of the elements of the cluster, there will be no effect on the particle motion, and hence no effect on the information content of the beamformer outputs. This seems to suggest that a modest enlargement of the receiving aperture, although it would certainly improve the directivity, might be of no aid in identifying the cluster structure. Yet, under some circumstances, that is definitely not true. If the beamformer outputs are seriously corrupted by measurement noise

of a sort that does not grow with the size of the receiving aperture, such as electrical noise, then its enlargement should increase the received signal energy, thereby improving S/N even though the enlargement has no effect on the particle motion. This improvement would certainly be beneficial for determining the direction of a solitary wave center, since in that instance the precision is limited only by measurement noise. But in the case of waves from a cluster, the analysis of particle motion might be limited more by its sheer complexity than by measurement noise, and a modest aperture enlargement would then be of no benefit.

It should be acknowledged that this presentation has ignored some acoustical details. We have assumed perfect transduction, and the distortion of particle motion caused by the physical presence of the array has not been considered. The particle motion discussed here is predicated upon hypothetical free field conditions, i.e., it is the motion at the measurement point in the absence of the array, but shielded by the even beamformer's directivity function. We have also used the terms plane wave and wave center despite their contradictory nature. This practice will be continued, under the assumption that the wave centers are so distant that the incident waves are effectively planar. Notice that setting

$$X = -c\bar{q}_1(t) \tag{71}$$

and

$$Y = q_2(t) \tag{72}$$

provides a display of particle velocity, which is just as useful for determining wave direction. For this reason, the beamformer outputs $\bar{q}_1(t)$ and $q_2(t)$ may be referred to as the velocity outputs.

The use of an oscilloscope display to reveal wave angle (using sum-and-difference beamformers) has been known since the 1940's,[8] and has been

discussed in at least one textbook.[13] But in its traditional form the display has a frequency dependent angular scale, and the connection between the display and acoustic particle motion has been ignored.

XII. ANALYSIS OF X-Y DISPLAY MOTION FOR MULTIPLE WAVES

Regardless of whether one constructs a particle displacement display or a particle velocity display, or merely connects the $\bar{q}_1(t)$ and $q_2(t)$ outputs of any odd-even beamformer pair to an X-Y display device with arbitrary scaling, a solitary incident wave will manifest itself as a straight line through the origin. If the display point (X,Y) is $(\bar{q}_1,q_2)$, then $\bar{q}_1(t)=R(\theta)q_2(t)$, with $R(\theta)$ given by Eq. (35), and the point lies on the line $X-RY=0$ at all times. The displayed point will trace out that line repeatedly with each oscillation of the incident wave. The line will tilt to the right or left of vertical in accordance with the mapping of incidence angle to display angle that is induced by the function $R(\theta)$ (see Fig. 5). The length of the line as projected onto the Y-axis represents the peak-to-peak amplitude of the output of the even beamformer, so it will be relatively independent of the angle of incidence so long as the ray path remains within the broadside window.

If two waves arrive at different times and different angles, then two lines will be traced in succession (see Fig. 6(a)). If (X_1,Y_1) denotes the coordinates of the displayed point during the arrival of the first wave and (X_2,Y_2) denotes those during the second, then $X_1-R_1Y_1=0$ and $X_2-R_2Y_2=0$ where R_1 and R_2 denote $R(\theta_1)$ and $R(\theta_2)$. But if the waves arrive simultaneously, yielding the superposition of coordinates $(X_S,Y_S)=(X_1+X_2,Y_1+Y_2)$, then the display point will not be confined to a line. Its coordinates (X_S,Y_S) will obey

$$X_S - R_1Y_S = \left(1-R_1R_2^{-1}\right)X_2 \tag{73}$$

and

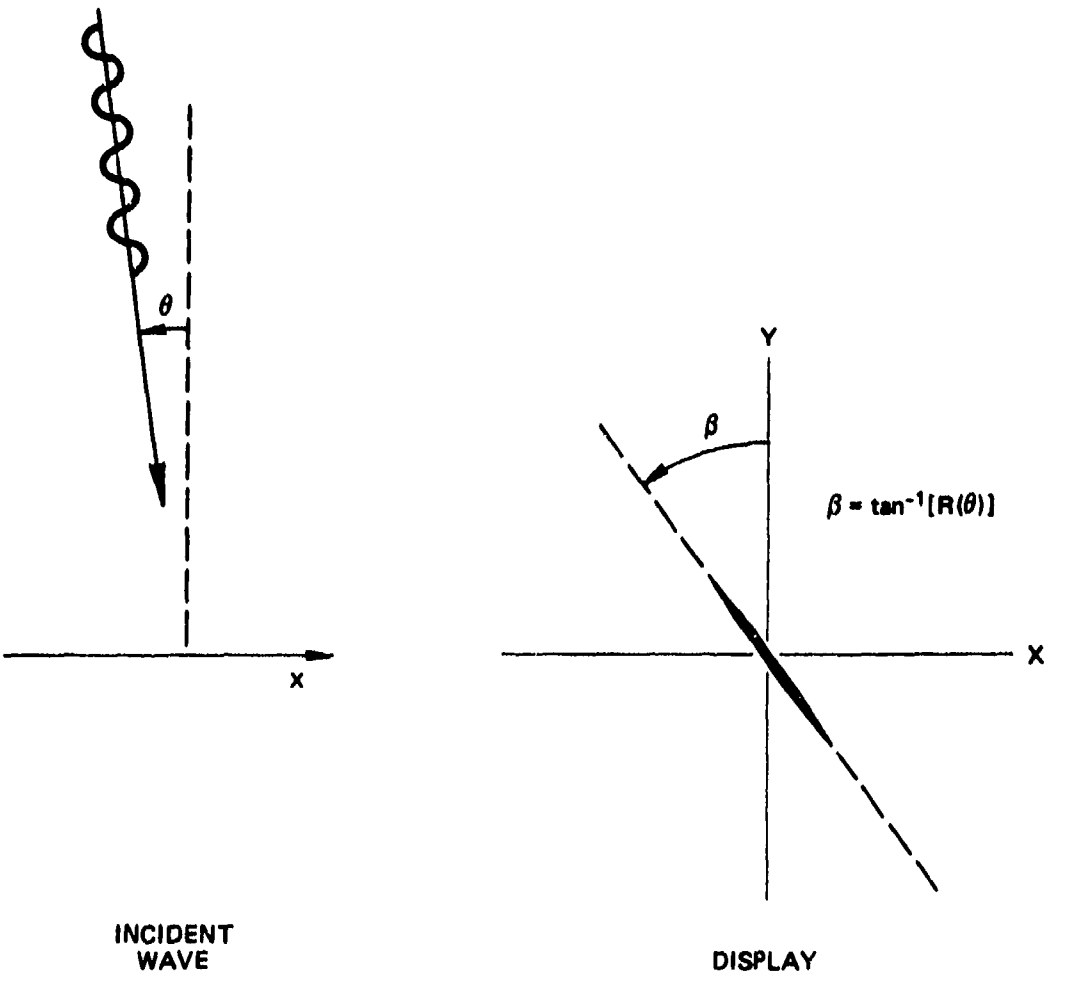

FIGURE 5
DISPLAY FOR A SOLITARY INCIDENT WAVE

ARL:UT
AS-82-785
TLH - GA
5 - 21 - 82

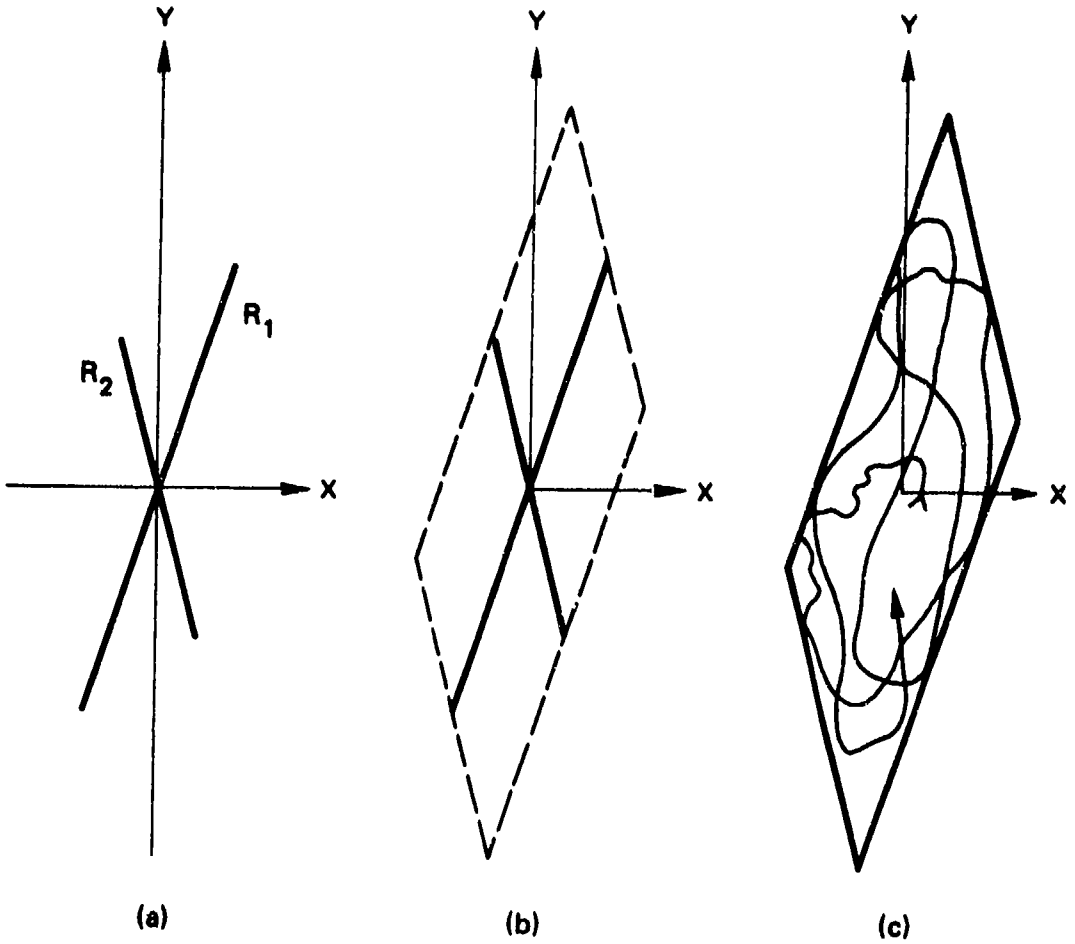

FIGURE 6
BOUNDARY PARALLELOGRAM

ARL:UT
AS-82-786
TLH - GA
5 - 21 - 82

$$X_S - R_2 Y_S = \left(1-R_2 R_1^{-1}\right) X_1 \quad , \tag{74}$$

and if we assume the subscripts have been chosen so that $R_2 > R_1$, then

$$\left(1-R_1 R_2^{-1}\right)\min\{X_2\} \le X_S - R_1 Y_S \le \left(1-R_1 R_2^{-1}\right)\max\{X_2\} \quad . \tag{75}$$

and

$$\left(R_2 R_1^{-1}-1\right)\min\{-X_1\} \le X_S - R_2 Y_X \le \left(R_2 R_1^{-1}-1\right)\max\{-X_1\} \quad . \tag{76}$$

These limits constrain the display point (X_S, Y_S) to the interior of a parallelogram. Two of its sides are parallel to the line $X-R_1Y=0$ with Y intercepts $Y_- = \left(1-R_1 R_2^{-1}\right)\min\{X_2\}$ and $Y_+ = \left(1-R_1 R_2^{-1}\right)\max\{X_2\}$, and the other two sides are parallel to the line $X-R_2Y=0$ with Y intercepts $Y_- = \left(R_2 R_1^{-1}-1\right)\min\{-X_1\}$ and $Y_+ = \left(R_2 R_1^{-1}-1\right)\max\{-X_1\}$. If wave 1 were extinguished then both bounds of Eq. (76) would become equal, and the display would collapse to a single line segment through the origin with slope R_2, its ends touching the parallogram boundaries. Similarly, if wave 2 were extinguished, the result would be a line with slope R_1, also touching the parallelogram boundaries (see Fig. 6(b)). These line segments bisect the sides of the parallelogram, and may be regarded as non-orthogonal but additive components of the display motion (see Fig. 6(c)).

If wave 2 is periodic with period T_2, then X_2 attains its maximum and minimum values at least once during each period, i.e., the display point touches both sides of the parallelogram defined by Eq. (75) during every time interval of duration T_2. Similarly, if wave 1 has period T_1, then the remaining two sides are touched at least once during that period. If both waves are periodic, then unless there is some coherence between the two waves, it is likely that enough different points of the bounding parallelogram will be touched to define it unambiguously after a brief interval of observation. Then R_1 and R_2 can be determined from the slopes of its sides, and if the angles of incidence lie within the range where $R(\theta)$ is monotonic, then θ_1 and θ_2 can be determined from R_1

and R_2 (see Fig. 7). It is thus possible to resolve both angles of incidence when the incident waves are periodic but not coherent, even when they arrive simultaneously. But it might be preferable just to separate them by using tuned filters.

More important is the case in which the two waves are coherent, being sinusoids of the same frequency. In this case, tuned filters would be of no use in separating the components. Both coordinates $X_S(t)$ and $Y_S(t)$ are sums of sinusoids of the same frequency; hence both reduce to single sinusoids, not necessarily of the same phase or amplitude. Anyone familiar with Lissajous patterns knows that the resulting display will be an ellipse. As a result of the properties discussed in the preceding paragraph, the ellipse must touch all four of the parallelogram's sides, i.e., it is inscribed in the parallelogram (see Fig. 8(a)). In the special case where the waves arrive in phase the ellipse degenerates to a straight line, which must be one of the diagonals of the parallelogram (in order to touch all four sides). The long and short diagonals thus represent constructive and destructive interference of the waves. Unfortunately, if the phase relationship of the incident waves remains steady, the ellipse will remain steady as well. A single inscribed ellipse is not sufficient to define the parallelogram. But if the relative phase between the wave components drifts while their amplitudes remain constant, then two or more inscribed ellipses will be seen and the boundary parallelogram will be revealed, i.e., the two wave angles will be resolved (see Fig. 8(b), (c), (d)). If, as in active sonar, the two waves are actually echoes from objects that are physically separate, then their relative phase may be altered by physical motion of the transmitter, the receiver, or the objects themselves, or by varying the operating frequency.

The inscribed ellipse interpretation has important implications for detecting the angle of a supposedly solitary wave that has been corrupted in some way. Suppose that, due to multipath (refractive or reflective) effects, what started out as a single wave arrives as two waves, at slightly different angles. Or, suppose that a weaker wave of

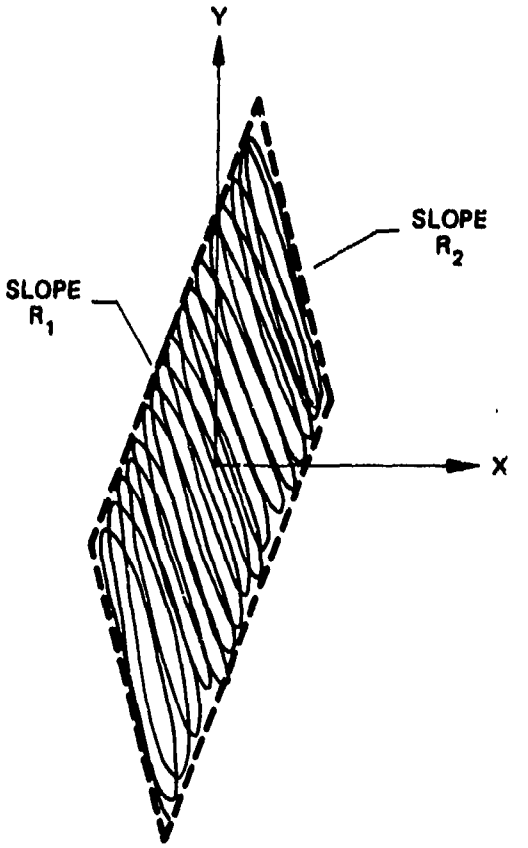

FIGURE 7
RESOLUTION OF DIRECTIONAL COMPONENTS
FOR WAVES OF DIFFERENT FREQUENCIES

ARL:UT
AS-82-787
TLH - GA
5 - 21 - 82

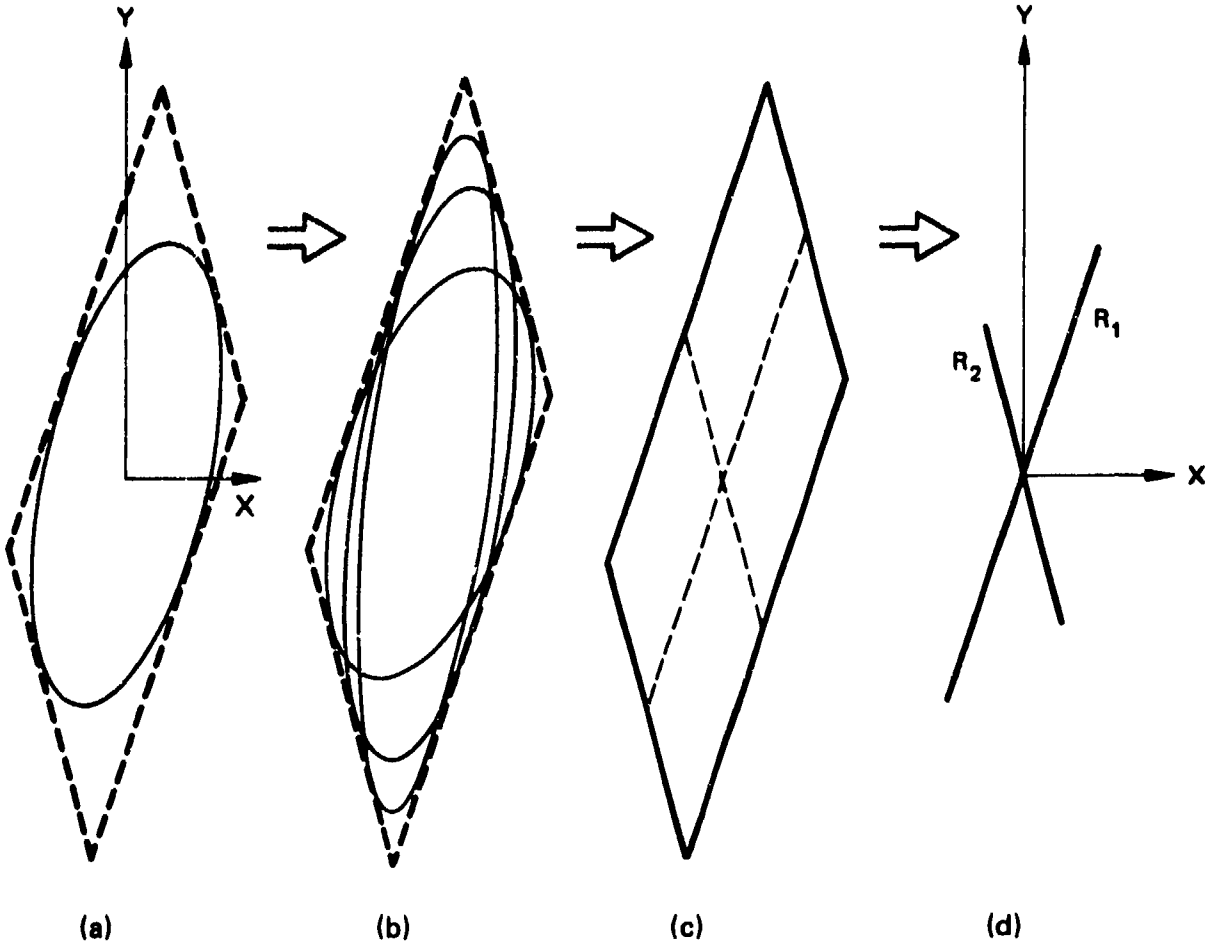

FIGURE 8
RESOLUTION OF TWO COMPONENTS
AT THE SAME FREQUENCY

ARL:UT
AS-82-788
TLH-GA
5-21-82

the same frequency arrives from a different wave center, perhaps due to reflection of a transmitted wave from a boundary. Given that the stronger wave produces a longer line segment component of the display than the weaker wave, it is clear (see Fig. 9) that the apparent direction of the wave, as interpreted by any reasonable characterization of the ellipse's angle of tilt, always lies within the longer wedge formed by the parallelogram diagonals. Thus the effect of the weaker wave is either to attract the apparent direction towards itself if the interference is constructive, or to repel it if the interference is destructive. In the latter case, the apparent direction does not lie between the actual wave centers. This phenomenon, whereby two wave centers conspire to appear elsewhere, is known as "glint" in the radar monopulse literature. Nevertheless, if the offending wave is significantly weaker, for example, if its contributed line segment component of the display is less than one third the length of that of the main wave, then the angular extent of the "wedge of uncertainty" is relatively small. In any case, parallelogram sketches are useful tools for predicting such effects. An even clearer picture of performance can be obtained from an X-Y oscilloscope with two oscillators set at slightly differing frequencies to simulate waves having a slowly varying phase difference. A means must be provided to additively mix the two signals into both channels of the oscilloscope.

If more than two waves arrive at the same time, the situation becomes rather more complicated. It is straightforward to show that the generalization of Eqs. (75) and (76) to N waves is

$$A_n \le X_S - R_n Y_S \le B_n \qquad \text{for } n=1,2,\ldots,N \quad , \qquad (77)$$

where A_n and B_n are the minimum and maximum values of

$$\sum_{m\neq n}^{N} \left(1-R_n R_m^{-1}\right) \quad .$$

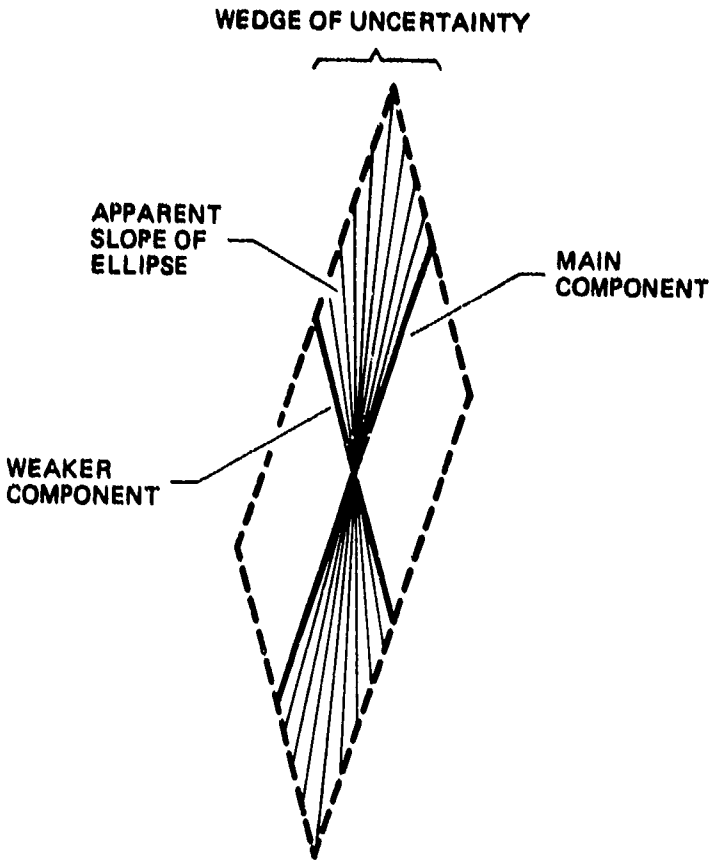

FIGURE 9
EFFECT OF A WEAKER COMPONENT

ARL:UT
AS-82-789
TLH - GA
5 - 21 - 82

These inequalities confine the display point to the interior of a polygon having 2N sides, grouped as N pairs of parallel sides. Unfortunately for N>2, the quantities A_n and B_n depend upon more than one wave, and even if each wave is periodic there is no guarantee that the display point will touch the corresponding sides during every period. But for every pair of sides of the boundary polygon that can be discerned, the corresponding slope R_n can be determined and the direction of that wave component resolved. The feasibility of such an approach for a given set of multiple waves is best explored via the oscilloscope method, or by a computer simulation.

A related method for resolving two monopulse radar targets has been developed by Sherman,[14] but that method is purely algebraic, and lacks the benefits of a geometrical interpretation.

Several investigators have analyzed monopulse radar behavior in the presence of multiple targets, employing statistical methods in most cases. Recall from Eq. (56) that a monopulse radar computes

$$r = \mathrm{Re}\left[\frac{Q_1}{Q_2}\right] \qquad \text{or} \qquad \mathrm{Re}\left[\frac{Q_1}{jQ_2}\right] \quad .$$

If the output phasors Q_1 and Q_2 represent the combined radar returns from many point scatterers, regarded as ideal point targets,

$$Q_1 = \sum_i Q_{1,i} \quad , \qquad Q_2 = \sum_i Q_{2,i} \quad , \tag{78}$$

then

$$r = \mathrm{Re}\left[\frac{\sum_i R_i Q_{2,i}}{\sum_i Q_{2,i}}\right] \quad , \tag{79}$$

where

$$R_i = \frac{Q_{1,i}}{Q_{2,i}} \qquad \text{or} \qquad R_i = \frac{Q_{1,i}}{jQ_{2,i}} \quad .$$

Note that each point target component would produce a real-valued ratio that accurately indicates its angle relative to broadside, i.e., $R_i = R(\theta_i)$. So,

$$r = \frac{\sum_i R(\theta_i) Q_{2,i}}{\sum_i Q_{2,i}} \quad . \tag{80}$$

Equation (80) may be used as the starting point for investigating the behavior of monopulse-type receivers for multiple targets, either via statistical methods or simulation.[10]

XIII. SLOPE DETECTION

Regardless of whether one really wishes to generate it, the concept of the X-Y display suggests good ways to extract wave angle from the odd-even beamformer outputs. As shown in the previous sections of this report, the beamformer outputs can be used to generate signals X(t) and Y(t) that, for a solitary incident wave in a perfect, noise-free environment, obey the straight line relationship $X(t)=R(\theta)Y(t)$ at all times, and θ can be determined from R within some monotonic range. We may even regard the observed factor R, the slope of the displayed line, to be a direct measure of wave angle in nonlinear "R units". (Although R will be referred to as the "slope", note that it is the slope of X versus Y rather than the more familiar Y versus X.) Noise, multipath, and extraneous wave sources may distort the line into something much more complex, such as an ellipse or a Brownian motion path. Neverthless, it is to be expected that the straight line component of the dominant wave will assert itself as a line of elongation, an axis of symmetry, or some other attribute that gives the display an identifiable slope. The problem of slope detection may be posed in a gross way as finding an estimate $\hat{R}$, such that

$$X(t) \cong \hat{R}Y(t) \quad . \tag{81}$$

If $\theta=0$, then under ideal conditions the display must be a vertical line with R=0. However, in the presence of random disturbances, the display will distribute itself symmetrically about the vertical axis, at least in a statistical sense, so that the product X(t)Y(t) averages to zero. If, on the other hand, the wave angle deviates from the broadside direction or, equivalently, if the line array is physically rotated, then the idealized straight line will have a nonzero slope R, i.e., it will rotate through an angle β, where $R=\tan\beta$. If the wave source is not so simple

and has an angular extent that produces a more complex display than a mere line, then the entire display pattern will rotate. There will be little or no discernible distortion associated with this rotation if the odd symmetric function $R(\theta)$, besides being monotonic, is approximately linear over an angular span that encompasses all of the wave sources which contribute significantly to the display pattern. Moreover, if statistically independent, Gaussian background noise corrupts the display variables $X(t)$ and $Y(t)$, and if these variables have been scaled for equal noise variance, then the display components contributed by this noise are statistically invariant with respect to rotation. Thus, under a broad class of circumstances, we are led to estimate the slope as

$$\hat{R} = \tan\beta \quad , \tag{82}$$

where β is the clockwise angle through which the display pattern must be rotated to decorrelate the coordinates of the display locus, i.e., β is the angle required to make

$$\mathrm{av}\{x(t)y(t)\} = 0 \quad , \tag{83}$$

where

$$\begin{bmatrix} x(t) \\ y(t) \end{bmatrix} = \begin{bmatrix} \cos\beta & -\sin\beta \\ \sin\beta & \cos\beta \end{bmatrix} \times \begin{bmatrix} X(t) \\ Y(t) \end{bmatrix} \quad . \tag{84}$$

The averaging operator denoted by $\mathrm{av}\{\cdot\}$ is quite general. Our subsequent developments will depend upon only two properties: (1) the averaging process must be a linear operation, and (2) the average of a nonnegative quantity must not be negative. Included, for example, is the case of an "average" formed by a low pass filter.

If the product $x(t)y(t)$ is formed from Eq. (84) and then substituted into Eq. (83), and the result divided by $\cos^2\beta$ and $\mathrm{av}\{Y^2(t)\}$, the following equation results:

$$(1-\tan^2\beta)r - (\tan\beta)p = 0 \quad , \tag{85}$$

where r and p are defined by

$$r = \frac{av\{X(t)Y(t)\}}{av\{Y^2(t)\}} \quad , \tag{86}$$

$$p = \frac{av\{Y^2(t)\} - av\{X^2(t)\}}{av\{Y^2(t)\}} \quad . \tag{87}$$

If $\hat{R}$ is substituted for $\tan\beta$, then a quadratic equation results:

$$r\hat{R}^2 + p\hat{R} - r = 0 \quad , \tag{88}$$

whose roots are

$$\hat{R}_1, \hat{R}_2 = \frac{-p \pm \sqrt{(p^2 + 4r^2)}}{2r} \quad , \tag{89}$$

where $\hat{R}_1$ denotes the root with the positively signed radical. Note that the product of the two roots is -1, i.e., each is the negative reciprocal of the other. This result should come as no surprise since negatively reciprocal slopes imply orthogonality, confirming that the rotated display remains just as uncorrelated if it is rotated an additional 90°. Of these two orthogonal choices for the apparent slope of the display, it is logical to select the one along which the display is most strongly distributed, and this can be accomplished by picking the root that has the same sign as av{X(t)Y(t)}, i.e., the same sign as r. But the radical term in Eq. (89) is always larger in magnitude than -p, so the sign of the numerator is controlled by the sign in front of the radical. Thus $\hat{R}_1$ is the root that always has the same sign as r, so we take

$$\hat{R} = \hat{R}_1 = -(\hat{R}_2) = \frac{2r}{p + \sqrt{(p^2+4r^2)}} \quad . \tag{90}$$

The quantity in brackets must lie between 0 and 2, as can be shown by some mildly tedious algebra that will only be outlined here: (1) the radical is larger in magnitude than p, so the number in brackets is non-negative. (2) From the two properties of av{·} given above, it is easily proven that $[av\{XY\}]^2$ never exceeds the product $av\{X^2\}av\{Y^2\}$, by mimicking the standard quadratic discriminant proof from basic statistics, wherein av{·} denotes expectation. (3) It follows, after some simple algebra, that the expression under the square root sign, p^2+4r^2, is bounded by $[(av\{x^2\}+av\{Y^2\})/av\{Y^2\}]^2$. (4) The sum of p and the square root of this bound is 2, so the quantity in brackets does not exceed 1.

Hence, the estimated slope $\hat{R}$ agrees in sign with, and equals or exceeds in magnitude, the coefficient r. Both quantities have a statistical interpretation. If the display comprises a set of points that would fit a straight line through the origin were it not for the corruptive effects of independent, Gaussian perturbations of zero mean, then r is the sampled coefficient of regression of X upon Y. If, in addition, the axes have been scaled for equal noise variance, then $\hat{R}$ is the maximum likelihood estimate of slope.[16]

When the display is dominated by waves (including directional noises) arriving at angles very near broadside, the X(t) signal will remain very weak, since it is derived from the output of the beamformer that has a broadside null. Expressed another way, the display will be tall and thin. Thus r will be quite small and p will approximate unity, so that r is an approximate estimate of R,

$$r \tilde{=} \hat{R} \tilde{=} R \quad . \tag{91}$$

If the beamformer outputs are dominated by sinusoidal waves whose spectral energy is concentrated at some frequency f_o, as in the case of active sonar, then X(t) and Y(t) will trace an ellipse, degenerating to

a straight line for a solitary incident wave having a well defined angle. If we represent the amplitude and phase of the sinusoids X(t) and Y(t) by phasors Z_x and Z_y, then if av{·} represents a long term arithmetic mean or a short term mean over an integral number of periods, then we see by analogy with the well known properties of voltage and current phasors in elementary electrical circuit analysis that

$$\text{av}\{X^2(t)\} = \frac{|Z_X|^2}{2} \quad , \quad \text{av}\{Y^2(t)\} = \frac{|Z_Y|^2}{2} \quad , \quad (92)$$

and

$$\text{av}\{X(t)Y(t)\} = \frac{\text{Re}\{Z_X Z_Y^*\}}{2} \quad . \quad (93)$$

It follows that

$$r = \frac{\text{Re}\{Z_X Z_Y^*\}}{Z_Y Z_Y^*} = \text{Re}\left[\frac{Z_x}{Z_y}\right] \quad (94)$$

and

$$p = 1 - |Z_X|^2 / |Z_Y|^2 \quad . \quad (95)$$

Equation (94) is completely equivalent to Eq. (56), allowing for harmless scaling; it is used in the monopulse radar literature to define slope detection for analytical purposes, although it is usually termed "angle detection" in recognition of the fact that the slope measures the wave's incidence angle in R units. However, the electronic circuitry used to compute the angle is often more indicative of Eq. (85).[6] Notice that r is the slope of a line drawn from the origin to the point of tangency of a horizontal line that just touches the top of the displayed ellipse (see Fig. 10). On the other hand, $\hat{R}$ is the slope of the "axis of

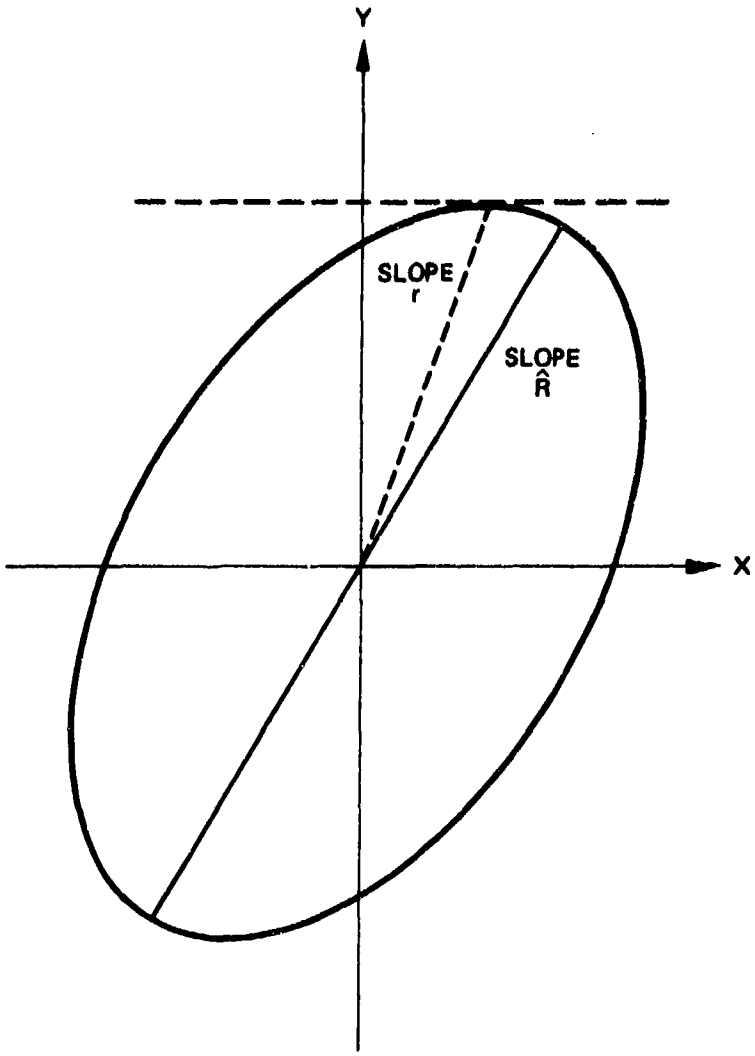

FIGURE 10

QUANTITIES r AND $\hat{R}$ FOR AN ELLIPTICAL DISPLAY

ARL:UT
AS-82-790
TLH-GA
5-21-82

decorrelation", i.e., it is the slope of the ellipse's major axis. To the author's knowledge, the only justification for using Eq. (94) ever given in the monopulse literature is that Z_X/Z_Y ought to be real, and that taking the real part is a reasonable way to force a real valued result when the sinusoids are not perfectly in phase.

It is evident from Eq. (85) that r is affected by a scaling of the coordinates X and Y in just the same manner as the slope of a line would be, i.e., it varies linearly with scaling of X and inversely with scaling of Y. The conversion of estimated slope to wave incidence angle would take any such scaling into account as a matter of course, so the detected wave angle would be invariant to any such scaling if r were used to estimate slope. But if $\hat{R}$ is used to estimate the slope, then the effect of scaling is somewhat different. If the X coordinates are scaled to a very small size, then p goes to 1 and $\hat{R}$ converges to r, and therefore produces the same detected wave angle. On the other hand, if the X coordinates are scaled to larger values, the detected angle may be substantially different, i.e., the detected angle using $\hat{R}$ is not invariant with respect to display scaling.

XIV. SUMMARY

The following concise summary of processing methods is presented as an aid to applications. The reader is referred to the main text for details.

Suppose Y(t) is driven by the output of a beamformer having even-symmetric shading, and X(t) is driven by the temporally integrated output of a beamformer having odd-symmetric shading. If both beams are formed from the same line array, then X(t) and Y(t) are related by a constant multiplicative factor, within certain restrictions. For a solitary sinusoidal wave incident at angle θ, they are related by

$$X(t) = R(\theta)\, Y(t), \tag{96}$$

where

$$R(\theta) = \frac{K_1(\theta, f_o)}{j2\pi f_o K_2(\theta, f_o)} \tag{97}$$

with $K_1(\theta,f_o)$ and $K_2(\theta,f_o)$ being the directivity functions of the odd and even beamformers at frequency f_o.

For a solitary wave of arbitrary spectrum incident at angle $\theta \ll 1$, i.e., very near broadside, Eq. (96) still holds with

$$R(\theta) = -\left(\frac{M_{1,1}}{M_{2,0}}\right) c^{-1} \sin\theta \quad , \tag{98}$$

where $M_{1,1}$ is the first moment of the odd beamformers aperture shading function and $M_{2,0}$ is the zeroth moment of the even shading function; i.e., it is the broadside sensitivity of the even beamformer.

If the even beamformer happens to be the Kerr-Murdock companion to the odd beamformer, then Eq. (96) holds for any incident wave spectrum and for all angles of incidence, with

$$R(\theta) = c^{-1} \sin\theta \quad . \tag{99}$$

The locus of points [X(t),Y(t)] is a straight line and R is its (X versus Y) slope, i e., the line makes an angle β with the vertical axis, where

$$\beta = \arctan R(\theta) \quad . \tag{100}$$

Over the domain for which $R(\theta)$ is monotonic, the angle of incidence can be determined from observation of R.

If several waves are incident at angles $\theta_1, \theta_2, \ldots$, then the locus is confined to the interior of a polygon that has two parallel sides for each of the slopes $R(\theta_1)$, $R(\theta_2), \ldots$, and the angle of a component wave can be determined (i.e., "resolved") whenever the corresponding polygon sides are observed. In particular, for two incident periodic waves the locus will be inscribed in a parallelogram.

The predominant slope of a locus corrupted by noise, multipath, or other disturbances may be estimated as

$$\hat{R}(\theta) = \frac{2r}{p + \sqrt{p^2 + 4r^2}} \quad , \tag{101}$$

where

$$r = \frac{A_{XY}}{A_{YY}} \quad , \tag{102}$$

$$p = \frac{A_{YY} - A_{XX}}{A_{YY}} \quad , \tag{103}$$

and A_{XY}, A_{XX}, and A_{YY} are the averaged values of XY, X^2, and Y^2, respectively. The average may be computed by a filter, for example. The number r is itself an estimate of the slope, and converges to $\hat{R}$ if both A_{XY} and A_{XX} are small compared with A_{YY}.

A computational transform method may also be used to process the beamformer outputs, as described in the main text of the paper.

APPENDIX
PERTURBATIONS OF APPARENT DIRECTION DUE TO PHASE FRONT DISTORTION

Let

$$w(r,t) = \mathrm{Re}\left\{W(r)\, e^{j2\pi f_o t}\right\} \tag{A.1}$$

be the total field at position r due to spherical, sinusoidal waves emanating from a collection of N targets. If the targets are located at distances $D_1, D_2, \ldots, D_N$ from the origin, lying in directions represented by unit vectors $u_1, u_2, \ldots u_N$, then the position of the ith target is represented by the vector $D_i u_i$. Let $W_i(r)$ denote the component of the complex envelope W(r) due to the ith target. Then it follows from the spherical nature of each wave tnat

$$W_i(r) = W_i(0)\left(\frac{D_i}{D_i - D_{ir}}\right) \exp\left(\frac{jD_{ir}2\pi f_o}{c}\right) \quad , \tag{A.2}$$

where D_{ir} denotes the distance between the point r and the ith target, $D_{ir} \triangleq |D_i u_i - r|$. The field in the vicinity of the origin may be found by expanding Eq. (A.2) to first order in the differential vector dr,

$$W_i(dr) = W_i(0)(1 + jK_i \langle u_i, dr \rangle) \quad , \tag{A.3}$$

where

$$K_i \triangleq \frac{2\pi f_o}{c} - \frac{j}{D_i} \tag{A.4}$$

and <a,b> denotes the inner product. Notice that K_i quickly converges to the real valued wave number constant, $2\pi f_o/c$, as the target distance increases. The total field due to the N targets is

$$W(dr) = \sum_i W_i(dr) = (1 + j\langle G, dr \rangle)W(0) \quad , \tag{A.5}$$

where

$$G \triangleq \frac{\sum_i W_i(0) K_i u_i}{\sum_i W_i(0)} \quad , \tag{A.6}$$

and we have made use of the fact that $W(0)=W_i(0)$. Contemplation of Eq. (A.5) leads to the conclusion that Re{G} is the gradient vector of the phase of the field in the vicinity of the origin, while $-|W(0)|$Im{G} is the gradient vector of the amplitude.

Let us consider some special cases. Suppose there is just one target at distance D_1 in direction u_1. Then $G=K_i u_i$, so the phase gradient is $(2\pi f_o/c)u_i$ while the amplitude gradient is $|W(0)|u_1/D_1$. Both gradient vectors point in the direction of the target, i.e., towards the source of the single spherical wave. The amplitude gradient is very weak for a distant target, but the phase gradient remains strong even at extreme distances.

The outcome is similar if there are N targets lying in the same direction, $u_1=u_2=,\ldots,u_N$, since G is then a scalar multiple of u_1. Both gradient vectors point in that direction and the magnitude of the phase gradient vector still approximates the wave number $2\pi f_o/c$, provided all of the targets are rather distant.

Now suppose there are N targets at different directions but with positions and phase characteristics that connive to make the spherical waves arrive at the origin in phase. Their shared phase component can then be canceled in the numerator and denominator of Eq. (A.6). In this case, the phase gradient is

$$\text{Re}\{G\} = \frac{2\pi f_o}{c} \frac{\sum_i |W_i(0)| u_i}{\sum_i |W_i(0)|} \quad . \tag{A.7}$$

This formula is convex with respect to the u_i's because the weighting coefficients are all positive; i.e., the phase gradient lies within a convex subset bounded by the vectors u_i, and points to a particular spot somewhere within the collection of targets, termed the "radar centroid" in monopulse literature. The amplitude gradient vector has a similar form:

$$-|W(0)|\,\mathrm{Im}\{G\} = |W(0)|\,\frac{\sum_i |W_i|\,u_i/D_i}{\sum_i |W_i|} \quad . \tag{A.8}$$

If all the targets are at roughly the same distance D_c, then the amplitude gradient is approximately $(c/2\pi f_o)|W(0)|D_c$ times the phase gradient, so they point in virtually the same direction.

When the spherical waves do not arrive in phase, the outcome is much more complicated. For active sonar applications, we are most interested in the case of a fairly distant collection of N targets that are clustered around an arbitrarily defined geometric center whose distance and direction from the origin are represented by D_c and the unit vector u_c, respectively. We assume the cluster has a limited downrange extent in the sense that D_i/D_c is extremely close to unity for all i, although the differences D_i-D_k are permitted to be much larger than the acoustic wavelength. In effect, this means $(2\pi f_o/c-j/D_c)$ can be substituted for the K_i's in Eq. (A.6), with the result that

$$G \tilde{=} K_c \sum_i (X_i+jY_i)u_i = K_c \sum_i Z_i u_i \tag{A.9}$$

to a very close approximation, where

$$X_i + jY_i = Z_i \triangleq \frac{W_i(0)}{W(0)} \quad , \tag{A.10}$$

and

$$K_c \triangleq \frac{2\pi f_o}{c} - \frac{j}{D_c} \quad . \tag{A.11}$$

Notice that $W(0) = \sum_i W_i(0)$ so $\sum_i X_i = 1$ and $\sum_i Y_i = 0$. If the target cluster has limited crossrange extent then the direction vectors u_i will all lie very close to u_c, and it follows that $\mathrm{Re}\{U\} \cong \sum_i X_i u_c = 1$, and $\mathrm{Im}\{U\} \cong \sum_i Y_i u_c = 0$, i.e., $U \cong u_c$. We can investigate the variation of U from this approximate value by setting $u_i = u_c + (u_i - u_c)$ in Eq. (A.10),

$$U = u_c + \tilde{U} \quad , \tag{A.12}$$

where the complex displacement vector $\tilde{U}$ is defined as

$$\tilde{U} \triangleq \sum_i Z_i (u_i - u_c) \quad . \tag{A.13}$$

Although u_c and the u_i's are real, and K_c is almost purely real, there is no simple rule for predicting the phase of the displacement vector $\tilde{U}$ because the complex ratios Z_i can have arbitrary phases. Even the direction of $\tilde{U}$ is uncertain, since it is a linear combination of the vectors $u_i - u_c$, which are likely to point in a variety of directions if the targets are clustered randomly about the geometric center.

The amplitude gradient vector points in the direction of $-\mathrm{Im}(G)$, which can be expressed using Eqs. (A.10) and (A.12) as

$$-\mathrm{Im}(G) \cong -\mathrm{Im}\{K_c U\} = \frac{u_c}{D_c} - \mathrm{Im}\{K_c \tilde{U}\} \quad . \tag{A.14}$$

Its direction is unpredictable due to the aforementioned uncertainty in $\tilde{U}$, which is likely to be the dominant factor since the term u_c/D_c is so small for a distant target. There is little that can be said about the amplitude gradient in this case, other than that it is likely to be very weak and may not point in the same direction as the phase gradient. Fortunately, the amplitude gradient is an unimportant factor here. Based upon radar experience, any odd-even beamformer pair, any monopulse radar, or virtually any tracking radar will characteristically perceive the target cluster to be in the direction of the phase gradient vector.

To get the phase gradient of the acoustic field we must take the real part of G,

$$\mathrm{Re}\{G\} = \mathrm{Re}\{K_c G\} = \left(\frac{2\pi f_o}{c}\right)(u_c + \mathrm{Re}\{\tilde{U}\}) + \frac{\mathrm{Im}\{\tilde{U}\}}{D_c} \quad . \qquad (A.15)$$

The last term can be neglected since the target cluster is distant, so the phase gradient points in the direction of $\mathrm{Re}\{U\}=u_c+\mathrm{Re}\{\tilde{U}\}$. We may think of it as pointing toward the apparent center of the target cluster, also termed the phase center in the radar literature. The apparent center is displaced from the geometric center in accordance with Eq. (A.15). The quantities Z_i in the definition of $\tilde{U}$ given by Eq. (A.13) express the fractional contribution of each target to the total field at the origin W(0), and can be expected to be of less than unit magnitude under normal circumstances. Due to the limited crossrange extent of the cluster, the vectors (u_i-u_c) are extremely small. Thus the vector $\tilde{U}$ must be of very small magnitude, and the apparent center is only slightly displaced from the geometric center. However, if the configuration and orientation of the cluster are such as to produce destructive interference of the component spherical waves at the origin, i.e., if the origin lies in the direction of a "null" in the radiation pattern of the cluster, then W(0) may be small, even zero. Under that circumstance, the fractions $Z_i=W_i(0)/W(0)$ may become very large, making the displacement vector $\tilde{U}$ quite significant. Indeed, the apparent center may jump entirely outside

the target cluster, and its location may fluctuate erratically when the cluster's orientation or configuration is changed. In early radar experience, this effect was often encountered when an aircraft target, which can be regarded as a cluster of point scatterers, performed rapid maneuvers or reacted to turbulent air. The effect may have first been attributed to brief flashes of specular radar reflection at different positions on the aircraft caused by rotation, thus explaining the use of the term glint. Theoretical analyses refute this explanation, however, revealing that the effect actually occurs when the received wave is weakest.

In summary, for the case of a distant cluster of N targets, the phase gradient of the total field at the origin points in the direction of the vector

$$\mathrm{Re}\{U\} = \sum_i X_i u_i \quad , \tag{A.16}$$

where u_i is the unit vector pointing toward the ith component target and the X_i is the real part of the complex ratio of its contributed field to the total field at the origin, with the X_i's obeying $\sum_i X_i = 1$. The vector Re{U} defines the apparent direction of the target cluster, i.e., the direction normal to the incident phase front. It is clear from Eq. (A.16) that the vector Re{U} will be attracted toward any exceptionally strong component of the cluster, and will at least point toward the interior of the cluster unless there is enough destructive interference of the waves that the glint phenomenon intrudes.

Consider which apparent directions are theoretically possible for a target cluster of a given geometry if we permit the phase and amplitude contributed by each component to be varied independently. We observe that, given any numbers a_i that have a positive sum S, we could theoretically adjust the phase and amplitude of each target's wave to give $W_i(0)=a_i$. Then $W(0) = \sum_i W_i(0) = S$, and $X_i=a_i(0)/S$. The apparent direction is that of the vector $\mathrm{Re}\{U\} = S^{-1} \sum_i a_i$. We thus conclude that

the apparent direction can correspond to any linear combination of the u_i's, provided the weighting coefficients have a positive sum. This conclusion is almost, but not quite, equivalent to saying that the apparent direction can lie anywhere in the subspace spanned by the u_i's. For a two-target cluster, the apparent direction can be anywhere in a half-plane containing the cluster whereas for a three-target cluster it can be anywhere in a half-volume which contains it. As an example, consider a two-target cluster. Although it may seem that there are four independent parameters to deal with, namely the real and imaginary parts of $W_1(0)$ and $W_2(0)$, it is really only necessary to consider $X_1=\mathrm{Re}\{W_1(0)\}$. The phase gradient is $2\pi f_0/c \times \mathrm{Re}\{U\}$, and $\mathrm{Re}\{U\}=X_1u_1X_2u_2=u_2+X_1(u_1-u_2)$, since $X_1+X_2=1$. So the apparent direction is that of a vector whose end point lies on the straight line passing through the end points of the unit vectors u_1 and u_2 that point toward the two component targets. If X_1 and X_2 are both positive, then that vector lies between u_1 and u_2, but if the waves destructively interfere, i.e., if X_1 and X_2 have opposite signs, then the vector's end point may lie elsewhere along the line. Notice that the phase gradient is of largest magnitude when its deviation is greatest, and when the destructive interference of the waves is most severe. Although this example illustrates that extreme deviations in apparent directions of a target cluster are possible, they are not necessarily probable. The use of the parallelogram sketching method as described in the main text of this report may be of value in predicting such effects.

The perturbations in the direction of the phase gradient are symptoms of "kinks" in the phase fronts that radiate from the cluster. Since they occur at points where destructive interference takes place, they must be aligned with the "null" directions in the directivity pattern of the cluster. The target cluster may be regarded as a transmitting array having an unusual shape. Figure A.1 shows phase fronts emanating from a two-target cluster with three-wavelength spacing, in which the emanated waves are of almost equal strength but are driven 180° out of phase.[15] Significant perturbations in the wave fronts are seen at only eight specific aspect angles. (Destructive interference

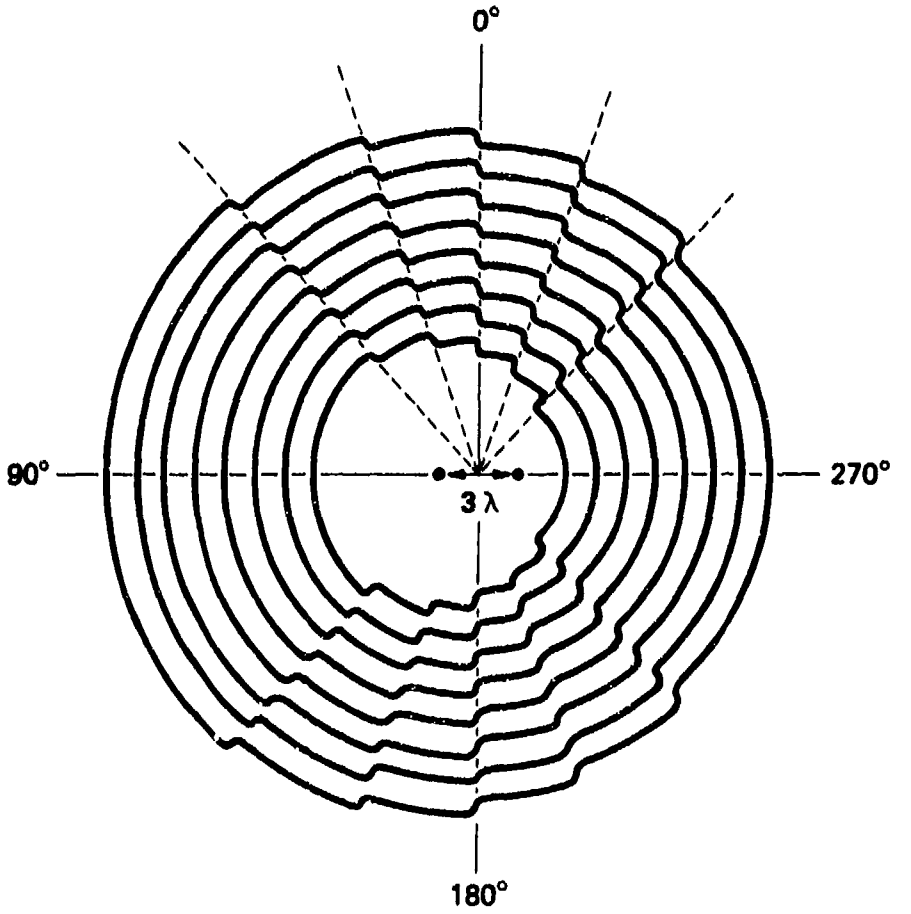

FIGURE A.1
DISTORTED PHASE FRONTS FROM TWO WAVE CENTERS SEPARATED BY THREE WAVELENGTHS AND DRIVEN 180° OUT OF PHASE

ARL:UT
AS-82-878
TLH-GA
6-7-82

also takes place at the end-fire angles, but without any attendant distortion in the phase front.) Note, however, that in the case of active sonar or radar illumination from a fixed direction, a simple rotation of the cluster does not produce an identical rotation of the kink pattern. The actual result is made more complicated by the changing phase relationship of the field incident upon the target components. Extensive measurements of the glint properties of specific cluster geometries (e.g., aircraft) have been performed in radar laboratories.

The treatment given in this appendix has used vectors rather than coordinate angles to represent target directions, but it may readily be verified that the bearing angle, relative to any "horizon," of the vector $\sum_i X_i u_i$, where the u_i's are almost collinear unit vectors and the numbers X_i sum to unity, is given to first order by $\sum_i X_i \theta_i$ where θ_i is the bearing angle of u_i. For the case of interest, $X_i = \mathrm{Re}\{W_i(0)/W(0)\}$ so the apparent bearing angle of the target cluster θ_c is given to first order by

$$\theta_c = \mathrm{Re}\left\{\frac{W_i(0)}{W(0)}\right\} \theta_i = \mathrm{Re}\left\{\frac{\sum_i \theta_i W_i(0)}{\sum_i W_i(0)}\right\} \quad . \qquad (A.17)$$

This expression is almost the same as that given in Eq. (79) for the sensing ratio used in monopulse radar, repeated here for convenience,

$$R = \frac{\sum_i R_i Q_{2,i}}{\sum_i Q_{2,i}} \quad . \qquad (A.18)$$

The two formulas are, in fact, equivalent for a small cluster near broadside. Recall that the R's measure the bearing angles in R units, which, for targets near broadside, give a linear measure of angle, and the constant of proportionality cancels in numerator and denominator. Furthermore, if the cluster is small with respect to the undulations of

the beam pattern of the even beamformer of an odd-even pair, then $Q_{2,1} \tilde{=} K_2(\theta_c)W_1(0)$, where $K_2(\theta_c)$ is the even directivity pattern function evaluated in the direction of the cluster, and this factor also cancels in numerator and denominator. The conclusion is that an odd-even beamformer pair perceives the cluster to lie in the direction of the phase gradient, perpendicular to the incoming phase front. The same conclusion applies to monopulse radar, as has been noted in the literature.[10,15]

REFERENCES

1. W. G. Bruner et al., "Radar and Navigational Systems," Electronic Designers Handbook, edited by L. J. Giacoletto (McGraw-Hill Book Co., Inc., New York, 1977).

2. P. Z. Peebles and R. S. Berkowitz, "Multiple-Target Monopulse Radar Processing Techniques," IEEE Trans. Aerospace & Electronics Systems, 845-854, (1968).

3. J. Capon, "High-Resolution Frequency-Wavenumber Spectrum Analysis," Proc. IEEE, 1408-1418 (1969).

4. J. S. Kerr and W. L. Murdock, "Relations Between the Far Field and the Illumination of Radar Apertures," GE Report No. 51-E-234, General Electric Company, 1 November 1951, Appendix B.

5. G. M. Kilpatrick, "Final Engineering Report on Angular Accuracy Improvement," General Electric Company Report, 1 August 1952, Appendix I. (See Ref. 9.)

6. D. R. Rhodes, Introduction to Monopulse (McGraw-Hill Book Co., Inc., New York, 1959).

7. Special Issue on Time Delay Estimation, IEEE Trans. Acoustics, Speech, & Signal Processing, July 1981.

8. National Defense Research Committee, "The Bearing Deviation Indicator" in "Underwater Sound Equipment II, Echo-Ranging Systems," Summary Technical Report of Division 6, NDRC, Office of Scientific Research and Development, Washington, D.C., 1946, Vol. 15, pp. 83-116.

9. D. K. Barton (ed.), Radars, Vol. 1, Monopulse Radar (Artech House, Inc., 1974).

10. R. A. Ross and M. E. Bechtel, "Scattering Center Theory and Radar Glint Analysis," IEEE Trans. Aerospace & Electronic Systems, 756-762 (1968).

11. I. Kanter, "Varieties of Average Monopulse Responses to Multiple Targets," IEEE Trans. Aerospace & Electronic Systems, 25-28 (1981).

12. D. K. Barton, "Accuracy of Monopulse Radar," IRE Proceedings of the 3rd National Convention on Military Electronics, 1959. (See Ref. 9.)

13. J. W. Horton, Fundamentals of Sonar (United States Naval Institute, Annapolis, Md., 1959).

14. S. M. Sherman, "Complex Indicated Angles Applied to Unresolvable Radar Targets and Multipath," IEEE Trans. Aerospace & Electronic Systems, 160-170, 1971.

15. D. D. Howard, "Radar Target Angular Scintillation in Tracking and Guidance Systems Based on Echo Signal Phase Front Distortion," Proceedings of National Electronics Conference, Vol. 15, 1959.

16. M. G. Kendall and A. Stuart, Chapter 29 of The Advanced Theory of Statistics (Charles Griffin & Co., Ltd., London).

17 May 1982

DISTRIBUTION LIST FOR
ARL-TM-82-10
UNDER CONTRACT N00024-79-C-6358, Task 8, Subtask 14
UNCLASSIFIED

Copy No.

Commander
Naval Sea Systems Command
Department of the Navy
Washington, DC 20362

1 Attn: D. Porter (Code 63R1)
2 A. Carpenter (PMS 407)
3 C. Smith (Code 63R)
4 E. Liszka (PMS 406)
5 J. Neely (PMS 409C)
6 F. Romano (Code 63R3)
7 B. Chapman (Code 63Z34)
8 L. Epperly (Code 63D)
9 R. Snuggs (PMS 409)
10 Library (Code 9961)

Commanding Officer
Office of Naval Research
Arlington, VA 22217

11 Attn: A. Ellenthorp (Code 220)
12 R. Obrochta (Code 230)
13 CAPT A. Gilmore (Code 220)
14 P. Rodgers (Code 425AC)
15 L. Hargrove (Code 412)

Commanding Officer
Naval Research Laboratory
Underwater Sound Reference Detachment
P. O. Box 8337
Orlando, FL 32856

16 Attn: J. Blue

Commanding Officer
Naval Ocean Research and Development Activity
NSTL Station, MS 39529

17 Attn: E. Chaika
18 B. Blumenthal

Defense Advanced Research Projects Agency
1400 Wilson Boulevard
Arlington, VA 22209

19 Attn: T. Kooij, TTO

Distribution List for ARL-TM-82-10 under Cont. N00024-79-C-6358, Task 8, Subtask 14

Copy No.

Naval Electronic Systems Command
Department of the Navy
Washington, DC 20360
20 Attn: R. Mitnik, Code 612

21 Commander
Naval Material Command
Department of the Navy
Washington, DC 20360

Commander
Naval Ocean Systems Center
Department of the Navy
San Diego, CA 92152
22 Attn: J. Reeves
23 R. Anderson
24 R. McLennan
25 H. Sexton

Commanding Officer
Naval Oceanographic Office
NSTL Station, Bay St. Louis, MS 39522
26 Attn: W. Jobst
27 G. Lewis

Commanding Officer
Naval Coastal Systems Center
Panama City, FL 32407
28 Attn: L. Flax
29 S. Richardson

Commander
Naval Surface Weapons Center
White Oak Laboratory
Silver Spring, MD 20910
30 Attn: Library

Superintendent
Naval Postgraduate School
Monterey, CA 93940
31 Attn: Library

32 Commanding Officer and Director
Defense Technical Information Center
Cameron Station, Building 5
5010 Duke Street
Alexandria, VA 22314

Distribution List for ARL-TM-82-10 under Cont. N00024-79-C-6358, Task 8, Subtask 14

Copy No.

Applied Physics Laboratory
University of Washington
1013 N.E. 40th Street
Seattle, WA 98105
33 Attn: Library

Applied Research Laboratory
The Pennsylvania State University
P. O. Box 30
State College, PA 16801
34 Attn: Library

Admiralty Underwater Weapons Establishment
Portland, Dorset DT5 2JJ
UNITED KINGDOM
35 Attn: R. Bugler
36 D. Weston
37 J. Willis

University of Rhode Island
Kingston, RI 02881
38 Attn: Prof. D. W. Tufts
39 Prof. L. Scharf

Yale University
New Haven, CT 06520
40 Attn: Prof. P. M. Schultheiss

Princeton University
Princeton, NJ 08540
41 Attn: Prof. S. Schwartz

University of Mississippi
University, MS 38677
42 Attn: Prof. L. W. Pearson

Electronic and Electric Engineering Division
University of Technology
Loughborough, Leicestershire
UNITED KINGDOM
43 Attn: R. Griffiths

Department of Physics
The University of Texas at Austin
Austin, TX 78712
44 Attn: W. Nolle
45 T. Griffy

Distribution List for ARL-TM-82-10 under Cont. N00024-79-C-6358, Task 8, Subtask 14

Copy No.

Department of Electrical Engineering
The University of Texas at Austin
Austin, TX 78712

46 Attn: E. Powers
47 F. Bostick
48 T. Itoh
49 E. Hixson

50 Office of Naval Research
Resident Representative
Room No. 582
Federal Building
Austin, TX 78701

51 Electroacoustics Group, ARL:UT

52 Signal Physics Group, ARL:UT

53 Environmental Sciences Group, ARL:UT

54 Sonar Engineering Group, ARL:UT

55 Physical Sciences Group, ARL:UT

56 Sonar Development Division, ARL:UT

57 Lewie M. Barber, ARL:UT

58 Garland R. Barnard, ARL:UT

59 George P. Coble, ARL:UT

60 Marshall E. Frazer, ARL:UT

61 Terry L. Henderson, ARL:UT

62 Robert E. Hollingsworth, ARL:UT

63 Arthur C. Holly, ARL:UT

64 Claude W. Horton, ARL:UT

65 John M. Huckabay, ARL:UT

66 John W. Maxwell, ARL:UT

67 Chester M. McKinney, ARL:UT

68 T. G. Muir, ARL:UT

Distribution List for ARL-TM-82-10 under Cont. N00024-79-C-6358, Task 8, Subtask 14

Copy No.	
69	S. Patrick Pitt, ARL:UT
70	Dennis R. Powell, ARL:UT
71	Robert H. Stokes, ARL:UT
72	Reuben H. Wallace, ARL:UT
73	Joseph F. Willman, ARL:UT
74	Gary R. Wilson, ARL:UT
75	Library, ARL:UT
76 - 96	SEG Reserve, ARL:UT